Neuroimaging of Subacute Brain Inflammation and Microstructural Changes Predicts Long-Term Functional Outcome after Experimental Traumatic Brain Injury

Missault, Stephan; Anckaerts, Cynthia; Blockx, Ines; Deleye, Steven; Van Dam, Debby; Barriche, Nora; De Pauw, Glenn; Aertgeerts, Stephanie; Valkenburg, Femke; De Deyn, Peter Paul

Published in:
Journal of Neurotrauma

DOI:
10.1089/neu.2018.5704

JOURNAL OF NEUROTRAUMA 36:768–788 (March 1, 2019)

DOI: 10.1089/neu.2018.5704

Neuroimaging of Subacute Brain Inflammation and Microstructural Changes Predicts Long-Term Functional Outcome after Experimental Traumatic Brain Injury

Stephan Missault,[1,2] Cynthia Anckaerts,[2] Ines Blockx,[2] Steven Deleye,[3] Debby Van Dam,[4] Nora Barriche,[1] Glenn De Pauw,[1] Stephanie Aertgeerts,[1] Femke Valkenburg,[4] Peter Paul De Deyn,[4] Jeroen Verhaeghe,[3] Leonie Wyffels,[3,5] Annemie Van der Linden,[2] Steven Staelens,[3] Marleen Verhoye,[2] and Stefanie Dedeurwaerdere[6]

Abstract

There is currently a lack of prognostic biomarkers to predict the different sequelae following traumatic brain injury (TBI). The present study investigated the hypothesis that subacute neuroinflammation and microstructural changes correlate with chronic TBI deficits. Rats were subjected to controlled cortical impact (CCI) injury, sham surgery, or skin incision (naïve). CCI-injured ($n = 18$) and sham-operated rats ($n = 6$) underwent positron emission tomography (PET) imaging with the translocator protein 18 kDa (TSPO) radioligand [^{18}F]PBR111 and diffusion tensor imaging (DTI) in the subacute phase (≤3 weeks post-injury) to quantify inflammation and microstructural alterations. CCI-injured, sham-operated, and naïve rats ($n = 8$) underwent behavioral testing in the chronic phase (5.5–10 months post-injury): open field and sucrose preference tests, two one-week video-electroencephalogram (vEEG) monitoring periods, pentylenetetrazole (PTZ) seizure susceptibility tests, and a Morris water maze (MWM) test. *In vivo* imaging revealed pronounced neuroinflammation, decreased fractional anisotropy, and increased diffusivity in perilesional cortex and ipsilesional hippocampus of CCI-injured rats. Behavioral analysis revealed disinhibition, anhedonia, increased seizure susceptibility, and impaired learning in CCI-injured rats. Subacute TSPO expression and changes in DTI metrics significantly correlated with several chronic deficits (Pearson's $|r| = 0.50–0.90$). Certain specific PET and DTI parameters had good sensitivity and specificity (area under the receiver operator characteristic [ROC] curve = 0.85–1.00) to distinguish between TBI animals with and without particular behavioral deficits. Depending on the investigated behavioral deficit, PET or DTI data alone, or the combination, could very well predict the variability in functional outcome data (adjusted $R^2 = 0.54–1.00$). Taken together, both TSPO PET and DTI seem promising prognostic biomarkers to predict different chronic TBI sequelae.

Keywords: diffusion tensor imaging; MRI; PET; positron emission tomography; post-traumatic epilepsy; TSPO

Introduction

Traumatic brain injury (TBI) is a major public health and socioeconomic problem, which affects all ages and populations throughout the world. TBI is defined as any kind of brain injury due to external force and is a leading cause of mortality and morbidity worldwide. It is commonly referred to as a silent epidemic, partly due to public unawareness of the major long-lasting consequences that can occur following TBI including post-traumatic epilepsy, cognitive problems, and psychiatric deficits.[1,2] Prognostic models have been developed to predict the outcome following TBI, but a major limitation in the construction of these models was that they only used mortality and unfavorable outcome (dead, vegetative state, and severe disability) as possible outcomes, although the prediction of the different sequelae that can develop following TBI remains unaddressed.[3,4] This dichotomization evidently leads to a loss of information and a reduced sensitivity of the prognostic models.[5] Moreover, these models use rather unspecific predictors such as age, motor score, and pupillary reactivity.[3,4] A more comprehensive approach to identify specific predictors may

[1]Experimental Laboratory of Translational Neuroscience and Otolaryngology, Faculty of Medicine and Health Sciences, [2]Bio-Imaging Lab, Faculty of Pharmaceutical, Biomedical and Veterinary Sciences, [3]Molecular Imaging Center Antwerp, Faculty of Medicine and Health Sciences, [6]Laboratory of Experimental Hematology, Faculty of Medicine and Health Sciences, University of Antwerp, Wilrijk, Belgium.
[4]Laboratory of Neurochemistry and Behavior, Institute Born-Bunge, University of Antwerp, Wilrijk, Belgium; Department of Neurology and Alzheimer Research Center, University of Groningen and University Medical Center Groningen (UMCG), Groningen, The Netherlands.
[5]Department of Nuclear Medicine, University Hospital Antwerp, Edegem, Belgium.

be to investigate the link between a potential prognostic biomarker that is linked to the underlying neurobiological response to TBI and the development of chronic deficits. Moreover, although the existing prognostic models have been shown to be of value for the classification of patients, great caution is required when applying them to determine the individual risk of a single patient.[6] The identification of specific prognostic biomarkers would be of major value to identify patients who will develop a certain chronic consequence. Additionally, they might provide insight into the underlying neurobiological mechanisms that give rise to the TBI-related sequelae and open new avenues toward treatment and possibly prevention of these secondary consequences.

Inflammation is a very important secondary injury mechanism in TBI. Upon initial injury, a neuroinflammatory response is elicited, which involves both resident and peripheral immune cells. This response is complex and can have both beneficial and detrimental consequences for the neurons, depending on the timing and the cell types involved, as well as the molecular context in which they act.[7,8] Several inflammatory mediators have been demonstrated to exhibit epileptogenic and ictogenic properties and might be involved in the development of post-traumatic epilepsy.[7] Neuroinflammation has also been demonstrated to play an important role in cognitive dysfunction and psychiatric deficits following TBI. Inhibition of subacute microglial activation and suppression of subacute release of pro-inflammatory cytokines and chemokines has been shown to improve the cognitive outcome following experimental TBI.[9–11] Acute inflammatory biomarker profiles in cerebrospinal fluid of TBI patients have been shown to predict the risk for developing depression.[12] Evidence suggests that TBI induces microglial priming, which renders microglia more susceptible to a secondary inflammatory stimulus. An exaggerated inflammatory response to a secondary insult has been shown to concur with cognitive impairment and depressive behavior.[13,14]

Positron emission tomography (PET) radioligands that bind to the translocator protein 18 kDa (TSPO), which is highly upregulated on the outer mitochondrial membrane of activated microglia (among other cell types), are ideally suited to assess brain inflammation *in vivo* and to investigate whether early inflammation following brain insults can act as a prognostic biomarker for the long-term functional outcome. We have recently shown that *in vivo* assessment of TSPO expression in the early phase following *status epilepticus* could predict the frequency of chronic spontaneous recurrent seizures and behavioral co-morbidities in a rat model of temporal lobe epilepsy.[15] Few *in vivo* imaging studies with TSPO radioligands have been performed in TBI models. Wang and colleagues reported a peak in TSPO ligand binding at 6 days after controlled cortical impact (CCI) injury, which decreased gradually to near normal levels at 28 days post-injury.[16] Yu and associates also observed a peak in TSPO ligand binding at one week after fluid percussion injury, which decreased during the next 8 weeks of observation.[17] However, a limitation of TSPO is the lack of cell specificity. Whereas TSPO is highly expressed by activated microglia, it is also upregulated in other activated immune-competent cells, including macrophages, astrocytes, neutrophils, and lymphocytes.[16–18] Although several studies in TBI animal models pointed to microglia/macrophages as the main cellular sources of the TSPO signal with an additional contribution of astrocytes, a contribution of neutrophils and lymphocytes cannot be excluded.[16,17,19]

Diffusion imaging has emerged as a very powerful tool to characterize microstructural changes in both gray and white matter following TBI. Both diffusion-weighted imaging (DWI) and diffusion tensor imaging (DTI) have been proven to be highly sensitive techniques to assess alterations in tissue microstructure and diffuse axonal injury after TBI.[20–23] The average diffusion (average of three diffusion co-efficients in three orthogonal directions) has been investigated as a potential prognostic biomarker of the long-term functional outcome following experimental TBI. Kharatishvili and co-workers showed that average diffusion in the ipsilesional hippocampus at both early and chronic time-points following lateral fluid percussion injury (FPI) correlated with pentylenetetrazole (PTZ)-evoked seizure susceptibility at 12 months post-injury.[24] In an extended re-analysis of these data, Immonen and colleagues observed that average diffusion in the perilesional cortex and thalamus at 2 months post-injury showed the highest predictive value for increased seizure susceptibility at 12 months post-injury.[25] In another study from Immonen and colleagues it was demonstrated that average diffusion in the ipsilateral hippocampus at 23 days following FPI correlated with Morris water maze (MWM) performance at 7 months post-TBI.[26] Frey and associates showed that the subacute apparent diffusion coefficient (DWI in one direction) in injured cortex after FPI correlated with chronic kainate-evoked seizure susceptibility.[27] Several clinical studies also indicate that DTI can be useful for the prognosis of TBI (reviewed by Irimia and colleagues[20]).

Bigger lesion volumes, determined by T_2-weighted magnetic resonance imaging (MRI), have been shown to be associated with a poorer outcome after TBI.[28]

In this study we have first of all investigated whether (1) subacute brain inflammation, assessed by *in vivo* PET imaging with the TSPO ligand [^{18}F]PBR111, (2) subacute microstructural changes, assessed by *in vivo* DTI, and (3) subacute lesion volume, assessed by T_2-weighted MRI, correlated with the different chronic sequelae that may occur following TBI, including psychiatric deficits, spontaneous recurrent seizures, increased seizure susceptibility, and visuospatial learning and memory deficits. Next, we have evaluated the sensitivity and specificity of these parameters in distinguishing between TBI animals with and without particular deficits. Finally, we have investigated whether PET data, DTI data, or lesion volume alone, or the combination of these assessments, could best predict the variability in the different functional outcome parameters.

Methods

Animals

Eighty-four male Sprague-Dawley rats were purchased from Envigo (previously Harlan Laboratories), The Netherlands. Animals were group-housed in a temperature- and humidity-controlled room on a 12-h light-dark cycle with standard food and water available *ad libitum* until the moment of electrode implantation. From that point onward, animals were single-housed. Animals were treated in accordance with the EU directive 2010/63/EU. Animal experiments were approved by the animal ethics committee of the University of Antwerp, Belgium (ECD 2012-62).

Study design

There were in total three cohorts of animals in this study. The first and main cohort (cohort 1) included animals that were subjected to subacute *in vivo* imaging and chronic behavioral testing, and electroencephalogram (EEG) monitoring following experimental TBI (CCI-injury). The second cohort of animals (cohort 2) was subjected to an open field test and seizure susceptibility test in the chronic period to confirm observations that were made in the first cohort of animals. The third cohort of animals (cohort 3) was sacrificed in the subacute period for histological purposes.

The study design of the longitudinal *in vivo* imaging and behavioral study (cohort 1) is shown in Figure 1. A total of eight naïve, seven sham-operated, and 19 CCI-injured rats were initially included in this cohort. Six sham-operated and 18 CCI-injured rats were subjected to *in vivo* imaging (PET/computed tomography [CT] and MRI) in the subacute phase following TBI. Naïve animals were not subjected to *in vivo* imaging. PET/CT imaging was performed at 7 and 21 days post-injury and MRI at 4 and 18 days post-injury. One sham-operated rat and one CCI-injured rat were scanned at the first time-point, but died before the second time-point. The sham-operated rat was included in the PET and DTI analysis to investigate differences in TSPO expression and DTI metrics between CCI-injured and sham-operated rats. The CCI-injured rat, however, died during the first PET/CT scanning session and was therefore excluded from the entire study (see below). Eight naïve, six sham-operated, and 18 CCI-injured rats (including all rats that had undergone *in vivo* imaging in the subacute phase) underwent behavioral testing in the chronic period (5.5–10 months post-injury). One sham-operated rat exhibited significantly enlarged ventricles and aberrant behavior compared with the other sham-operated rats and was excluded from the entire study (see below). In total, 17 CCI-injured rats were used to investigate a possible relationship between early brain inflammation, microstructural changes and lesion volume, and chronic behavioral deficits. Finally, some rats lost their electrode assembly during the study. EEG data from these rats were included up to the point that they lost their electrode cap.

Cohort 2 consisted of nine naïve, 10 sham-operated, and 10 CCI-injured rats, which were subjected to an open field test at 2 months post-injury and a PTZ seizure susceptibility assay at 6 months post-injury to corroborate observations from cohort 1.

Cohort 3 consisted of four naïve, five sham-operated, and 12 CCI-injured rats. They were sacrificed at 7 days post-injury for histological purposes.

Controlled cortical impact-induced traumatic brain injury

CCI-injury was performed as previously described.[29] Eight-week old rats (mean ± standard error of the mean [SEM]: 281 ± 3 g) were anesthetized with isoflurane in oxygen (5% induction, 2.5% maintenance; Forene; Abbott, Belgium). During the surgery, the animal was kept warm by means of a temperature-controlled heating pad. A craniectomy of 5 mm diameter was performed with a trephine over the left parietal cortex (midway between bregma and lambda, bordering the lateral edge) without damaging the dura. CCI was done with the Leica Impact One device (Leica Biosystems, US) using the following parameters: flat tip of 3 mm diameter, impact angle 18 degrees, impact velocity 4 m/sec, depth of penetration 2.5 mm, dwell-time 500 msec ($n = 19$). After impact, the cranial window was sealed with a piece of plastic, and skin sutured. Sham-operated animals were subjected to the same surgery, but were not exposed to impact ($n = 7$). Because previous work has shown that craniotomized animals can display behavioral deficits compared with naïve animals, naïve rats were included in this study as well.[30] Naïve animals received anesthesia and a skin incision, but no craniectomy ($n = 8$). Naïve rats were treated in exactly the same way as sham-operated and CCI-injured rats, but did not undergo *in vivo* imaging.

PET imaging with [^{18}F]PBR111

Radiosynthesis of the TSPO radioligand [^{18}F]PBR111 was performed on a FluorSynton I automated synthesis module (Comecer, The Netherlands) according to Bourdier and colleagues.[31] PET scans were performed on an Inveon PET/CT scanner (Siemens Preclinical Solution, US) as previously described with a few minor modifications.[15] Rats were anesthetized with isoflurane in oxygen (5% induction, 2–2.5% maintenance; Abbott, Belgium), after which 8.6 ± 0.4 MBq radiotracer (molar activity: 149.8 ± 11.0 GBq/μmol) was administered by tail vein injection in a volume of 0.5 mL. During the uptake period of 45 min, the animal remained anesthetized and was kept warm by means of a temperature-controlled heating pad. Next, animals were subjected to a static PET scan of 15 min, followed by a 7-min CT scan. At 50 min post-injection, an arterial blood sample was collected from the tail artery for radiometabolite analysis according to Katsifis and associates.[32] During the scanning session, breathing rate and temperature were constantly monitored (Minerve, France) and maintained within normal physiological ranges. The temperature of the animal was maintained by supplying heated air through the imaging cell. PET images were reconstructed using a two-dimensional (2D) ordered subset expectation maximization algorithm (four iterations, 16 subsets) after Fourier rebinning.[33,34] Normalization, dead time, random, CT-based attenuation, and scatter corrections were applied.

Image processing was done using PMOD version 3.3 (PMOD Technologies, Switzerland). The CT images were co-registered to three-dimensional (3D) T_2-weighted MR images that were acquired earlier that week (see below) by manually guided automatic rigid matching. This CT to MR transformation was used to co-register the PET images to the MR images. The following volumes of interest (VOIs) were manually drawn on each individual 3D MR scan: lesion (hyperintense on the T_2-weighted MR image), perilesional cortex, contralateral cortex, ipsilesional hippocampus, and contralesional hippocampus. VOI statistics in kBq/cc were generated and used to calculate the standardized uptake values (SUV: average tissue radioactivity concentration [kBq/cc]/injected dose [kBq]/body weight [g]). For correlation analyses, we also calculated the relative change in SUV over time in CCI-injured rats according to the following formula:

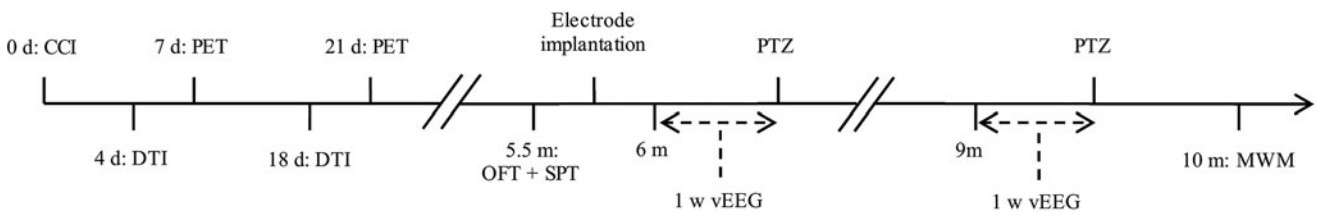

FIG. 1. Study design. Time line of the tests of the main cohort of animals (cohort 1). Young adult male Sprague-Dawley rats were subjected to controlled cortical impact (CCI) injury, sham surgery, or skin incision. CCI-injured ($n = 18$) and sham-operated rats ($n = 6$) underwent positron emission tomography (PET) imaging with the translocator protein (TSPO) radioligand [^{18}F]PBR111 at 7 days and 21 days post-injury, as well as diffusion tensor imaging (DTI) at 4 days and 18 days post-injury. CCI-injured ($n = 18$), sham-operated ($n = 6$), and naïve rats ($n = 8$) were subjected to chronic behavioral testing: an open field test (OFT) and sucrose preference test (SPT) at 5.5 months post-injury, one-week continuous video-electroencephalogram (vEEG) monitoring periods at 6 and 9 months post-injury, followed by pentylenetetrazole (PTZ) seizure susceptibility assays, and a Morris water maze (MWM) test at 10 months post-injury.

$$\%\ change = \left(\frac{SUV\ at\ 21\ days - SUV\ at\ 7\ days}{SUV\ at\ 7\ days}\right) * 100$$

One CCI-injured rat died during the CT scan at the first time-point. This rat was excluded from the entire study. One sham-operated rat got an infection of the tail following the first scanning time-point and was subsequently sacrificed. These rats were not scanned at the second time-point (neither PET/CT or MRI).

In vivo MRI: DTI and 3D T_2-weighted anatomical MRI

Rats were anesthetized with isoflurane in a mixture of O_2 (30%) and N_2 (70%) (5% induction, 2–2.5% maintenance; Abbott, Belgium). Breathing rate and blood oxygenation were monitored constantly using a pressure sensitive pad and a pulse oximeter (MR-compatible Small Animal Monitoring and Gating System, SA Instruments, Inc., US),and maintained between normal physiological ranges. The temperature of the animals was monitored by means of a rectal probe and maintained at 37 ± 0.5°C through a feedback-controlled warm air system (MR-compatible Small Animal Heating System, SA Instruments, Inc., US).

Data were acquired on a 7T PharmaScan with Paravision 5.1 software using a standard Bruker cross-coil set-up with a quadrature volume coil and a quadrature surface coil designed for rats (Bruker, Germany). The rat's head was immobilized in an MR-compatible stereotaxic device using blunt earplugs and a tooth bar. Three orthogonal multi-slice turbo rapid acquisition with relaxation enhancement (RARE) T_2-weighted images were acquired to ensure consistent slice positioning between DTI data of different animals. A field map was acquired to measure field homogeneity, followed by local shimming, which corrects for the measured inhomogeneity in a rectangular volume within the brain. Coronal diffusion-weighted (DW) images were acquired with a two-shot spin-echo echo planar imaging (SE-EPI) sequence with 60 optimally spread diffusion gradient directions. Fifteen non-DW b_0 images (b-value0 s/mm^2; 5 b_0 per 20 DW images) were acquired. The imaging parameters were: repetition time (TR) 7500 msec, echo time (TE) 26 msec, diffusion gradient pulse duration δ 4 msec, diffusion gradient separation Δ 12 msec, b-value 800 s/mm^2, 20 slices of 0.7 mm (limited to cerebrum), 0.1-mm slice gap, and scan duration approximately 20 min. The field of view (FOV) was 30×30 mm^2 and the matrix size 128×128, resulting in pixel dimensions of 0.234×0.234 mm^2. Following DTI, a 3D RARE T_2-weighted scan was acquired with the following parameters: TR 3185 msec, TE 11 msec (TE_{eff} 44 msec), RARE factor 8, 2 averages, FOV $29.0 \times 16.0 \times 10.2$ mm^3, acquisition matrix $256 \times 64 \times 50$, spatial resolution $0.113 \times 0.250 \times 0.204$ mm^3, and scan duration approximately 45 min.

DTI processing. Image processing was performed with SPM12 in MATLAB 2014a (MathWorks, US). First, images were realigned to correct for subject motion using the diffusion toolbox in SPM12. A rigid registration was performed between the b_0 images, which was followed by an extended registration taking also all DW images into account. Next, the diffusion tensor was estimated and the DTI parameter maps were computed (i.e., fractional anisotropy [FA], mean diffusivity [MD], axial diffusivity [AD], and radial diffusivity [RD]). Finally, the DTI parameter maps were smoothed in plane using a Gaussian kernel with full width at half maximum (FWHM) of twice the voxel size (FWHM $0.468 \times 0.468 \times 0.800$ mm^3). Regions of interest (ROIs; lesion, perilesional cortex, contralateral cortex, ipsilesional hippocampus, and contralesional hippocampus) were manually drawn in Amira 5.4.0 on the average b_0 (T_2-weighted) image of each animal and then adjusted on the individual FA and MD maps to ensure exclusion of white matter and ventricles. For each ROI, the mean value of the different DTI parameters was extracted in Amira 5.4.0. For correlation analyses, the relative change in DTI metrics over time in CCI-injured rats was calculated analogous to the percent change in [^{18}F]PBR111 SUVs above.

Volumetric analysis. As mentioned above, the lesion (edema) at 4 and 18 days was manually delineated on each individual 3D T_2-weighted MRI scan using PMOD version 3.3. In addition, we calculated the relative change in lesion volume over time in CCI-injured rats analogous to the percent change in [^{18}F]PBR111 SUVs and DTI metrics above. These measurements were used for correlation analyses with chronic deficits.

One sham-operated rat exhibited significantly larger ventricles at the first scanning time-point as compared with the other sham-operated rats (significant outlier) and showed a worse performance in several behavioral assays than the other sham-operated rats. This rat was excluded from the entire study. Spontaneous congenital hydrocephalus has been reported in this and other rat strains.[35]

Long-term outcome

Open field test. An open field test was performed to explore the presence of anxiety or disinhibition in CCI-injured rats. Cohort 1 (which included the animals that were subjected to *in vivo* imaging) was subjected to this test at ca. 5.5 months post-injury. Cohort 2 was subjected to this test at 2 months post-injury. Animals were placed in the periphery of a well-lit square arena ([48 × 48] cm^2) and allowed to explore the novel environment for 10 min. During this trial, animals were video-tracked with EthoVision XT software (version 10.0, Noldus, The Netherlands). For analysis, the arena was divided in a central zone (inner square, 24×24 cm^2) and a peripheral zone. The following parameters were calculated: latency to first entry in central zone, number of transitions from periphery to center, percent time spent in center, percent distance moved in center, total distance moved, and mean velocity.

Sucrose preference test. A sucrose preference test was done in cohort 1 at ca. 5.5 months post-injury to assess the presence of anhedonia in the CCI-injured rats. The test was performed as previously described.[36] Briefly, animals received two drinking bottles, one filled with water and one with 2% sucrose solution. After 48 h of habituation, the percent sucrose preference and total fluid intake were calculated over a test period of 24 h.

Video-EEG: spontaneous recurrent seizures and seizure susceptibility

Electrode implantation. All animals were implanted with six epidural screw electrodes as described before,[37] however, with a different positioning. One electrode was implanted rostral to the lesion over the left cortex (between bregma and lesion), two electrodes were implanted over the right cortex: one contralateral to the first electrode and the other opposite to the core of the lesion near the sagittal midline, one electrode was positioned over the left frontal lobe, and two more over the occipital lobe. Electrodes were fixed into a plastic plug (Bilaney Consultants, Plastics One, UK) and secured to the skull using dental cement (Simplex Rapid, Kemdent, UK; Durelon, 3M ESPE, US) and additional anchor screws. Animals were allowed to recover for at least one week before recording started.

Recording. Animals from cohort 1were subjected to continuous video-EEG (vEEG) recording for two periods of one week, once at 6 months post-injury and once at 9 months post-injury. The week of recording spontaneous epileptiform activity and seizures was each time followed by a PTZ seizure susceptibility test (see below). Animals were connected to a digital EEG acquisition system (Ponemah P3 Plus, Data Sciences International, US) through a cable system as previously described.[37] EEG was recorded from the electrode rostral

to the lesion and the contralateral electrode. The occipital electrodes were used as reference and ground electrodes. Due to limited capacity of the recording system, only four out of the eight naïve animals were subjected to continuous vEEG recording at the 6-month time-point. For the same reason, the CCI-injured rat and sham-operated rat that were not subjected to *in vivo* imaging did not undergo vEEG recording at this time-point. Between the 6-month and 9-month time-points, several animals lost their electrode assembly (4/8 naïve, 1/6 sham, 11/18 CCI). Hence, fewer rats underwent vEEG recording at the 9-month time-point.

Analysis. Video-EEG data were analyzed manually using NeuroScore 3.0 (Data Sciences International, US) as described before.[37] For the analysis of the spontaneous epileptiform activity and seizures, we quantified the number and duration of epileptiform discharges (EDs) and seizures per day, as well as the duration of all epileptiform activity (EDs + seizures) per day. An ED was defined as a high-amplitude (equaling at least 2 times the baseline amplitude) rhythmic discharge containing spikes and/or uniform sharp waves, lasting ≥1 sec but <5 sec. Most of the observed events were either spike-wave discharges or high-voltage rhythmic spike discharges. A similar event that lasted >5 sec was defined as a seizure. Video-analysis allowed us to classify seizures as purely electrographic events or behavioral seizures, which were scored according to a modified Racine scale as described before.[38] In this study, rats were considered epileptic if they experienced two or more unprovoked convulsive seizures (S3–5).[39]

PTZ-evoked seizure susceptibility test. Animals were injected subcutaneously (s.c.) with a single subconvulsive dose (25–30 mg/kg) of PTZ, after which they underwent 1 h of vEEG recording, a protocol adapted from Kharatishvili and colleagues.[24] For this test, we also quantified the number of spikes, in addition to EDs and seizures. We calculated the latency to first spike, first ED, first seizure (purely electrographic or behavioral) and first convulsive seizure, as well as the number of spikes, EDs, seizures (purely electrographic and behavioral), and convulsive seizures, and finally also the total duration of EDs, all seizures, and convulsive seizures. At 6 months post-injury, rats from cohort 1 received 25 mg/kg PTZ s.c.. Due to the low occurrence of convulsive seizures following this dose and previous reports in the literature that observed a more pronounced difference in the occurrence of convulsive seizures between TBI and control rats with a 30 mg/kg dose,[24,40] we decided to administer 30 mg/kg PTZ s.c. in cohort 1at 9 months post-injury. Three rats lost their electrode assembly during the PTZ tests (one CCI rat and one naïve rat at 6 months, one CCI rat at 9 months). They were excluded from the analysis of number of spikes, EDs, and seizures, but included in the analysis of latency to first spike, ED, and seizure (if recorded). For uniformity/standardization, all animals received PTZ injections at both 6 and 9 months, even if the animals had previously lost their electrode assembly and no EEG recording could be obtained. However, these were not included in the analysis. A PTZ test was also performed in cohort 2 at ca. 6 months post-injury, using the 30 mg/kg PTZ dose.

Morris water maze test. Rats from cohort 1 were subjected to a MWM test at ca. 10 months post-injury to investigate the extent of visuospatial learning and memory deficits in the CCI-injured rats. The test was performed as previously described.[41] The experimental set-up consisted of a circular pool (150 cm diameter) filled with white opaque water (kept between 20 and 24°C), containing a submerged round platform (15 cm diameter) and surrounded by visual cues. Prior to the test, rats were dyed black with a non-toxic hair dye to provide contrast with the white pool for video-tracking purposes (EthoVision XT 10.0, Noldus, The Netherlands). The test consisted of a training period (acquisition) of 8 days with the platform fixed in one place, and a probe trial (retention) during which the platform was removed from the swimming pool. Every training day consisted of four trials of maximally 120 sec each, with the rat starting from a different position for each trial (15 min inter-trial interval, semi-random order for each training day). If the rat could not locate the platform, it was placed on the platform for approximately 10 sec before being returned to its home cage. A learning curve was plotted for escape latency and path length to platform (sum of the four daily trials). In addition, we calculated the mean velocity. Four days after finishing the 8-day training period, the platform was removed and a probe trial of 100 sec was performed. We calculated the percent time spent in the target quadrant (i.e., the quadrant that previously contained the platform), as well as the number of crossings through the previous platform position.

Histology

Tissue collection. At 7 days post-injury, animals were sacrificed by decapitation. Brains were immediately resected and snap-frozen in ice-cold isopentane (3 min at −35°C) on dry ice. Brains were stored at −80°C until sectioning. Serial coronal cryosections (20 μm) were collected in triplicate at −2.92 mm from bregma (sections containing lesion core and dorsal hippocampus).

Immunohistochemistry

CD11b staining. Tissue sections were stained for CD11b, which is expressed by microglia/macrophages. Sections were stained as described before[42] with a few modifications. Sections were dried at room temperature for 5 min, followed by fixation with 4% paraformaldehyde. After washing with phosphate buffered saline (PBS), endogenous peroxidase and proteins were blocked with 3% H_2O_2 in dH_2O for 5 min and 3% normal horse serum (NHS) in PBS for 10 min. Sections were incubated overnight with mouse anti-CD11b antibody (AbD Serotec, UK; 1/1000) in antibody diluent, consisting of 0.1% bovine serum albumin, 0.2% Triton X-100, 2% NHS, and 1% milk powder in PBS. The following morning, sections were rinsed with PBS and incubated for 1 h with peroxidase-conjugated donkey anti-mouse IgG antibody (Jackson ImmunoResearch Laboratories, UK; 1/500) in antibody diluent. 3,3'-diaminobenzidine was used for colorimetric detection. After 10 min, the reaction was stopped with dH_2O, after which the sections were gradually dehydrated and cover-slipped.

GFAP staining. Tissue sections were stained for GFAP, which is expressed by astrocytes. The staining protocol was similar to the one for CD11b staining with a few exceptions. For blocking of endogenous proteins, a solution containing 3% normal goat serum (NGS), 1% milk powder, and 0.2% Triton X-100 in PBS was used for 1 h. Sections were incubated overnight with rabbit anti-GFAP antibody (Dako, Agilent Technologies, Belgium; 1/1000) in antibody diluent, containing 10% NGS and 1% milk powder in PBS. Sections were incubated with peroxidase-conjugated goat anti-rabbit antibody (Jackson ImmunoResearch Laboratories, UK; 1/500) in antibody diluent.

Analysis of CD11b and GFAP staining. Analysis was performed as described before.[29] Images were obtained with a NanoZoomer-XR slide scanner (Hamamatsu, Japan) equipped with a 20× objective and analyzed with ImageJ software. Images were transformed to 8-bit images and a threshold was set to select specifically stained cells from background staining. The area fraction, that is, the percent area of the ROI that consists of positively stained cells (microglia/macrophages or astrocytes) (as set by the threshold), was calculated for the following ROIs: perilesional and contralesional cortex, ipsi- and contralesional hippocampus. A higher area fraction reflects a higher density of CD11b-positive microglia/macrophages or GFAP-positive astrocytes in this ROI. All ROIs were outlined manually in triplicate samples.

In vitro autoradiography with TSPO radioligand [^{3}H]PK 11195. *In vitro* autoradiography with TSPO radioligand [^{3}H]PK 11195 was performed exactly as described before[37] with two exceptions: Sections were incubated with radiotracer for 1 h and exposed on films for 6 weeks.

Statistical analysis

Normal distribution of the data was tested using the D'Agostino-Pearson omnibus normality test. Outlier analyses were performed with the ROUT test. For the analysis of the open field test, sucrose preference test, spontaneous epileptiform activity and seizures at each time-point, seizure susceptibility tests and probe trial of the MWM test, we used Kruskal-Wallis tests to compare the three study groups (naïve, sham, CCI) and Dunn's multiple comparisons test as post hoc test. When pooling all controls (naïve + sham), we used Mann-Whitney U tests to compare the two groups (control, CCI). For correlation analyses, we used the Pearson correlation test. Chi-square tests for trend were performed to investigate whether the occurrence of convulsive seizures in the PTZ tests was associated with injury (naïve, sham, CCI). For receiver operater characteristic (ROC) curve analysis, CCI-injured animals were divided into two groups for each behavioral outcome parameter: CCI-injured rats with and without a deficit. Depending on the nature of the response, CCI-injured rats with a value higher than the mean + 2 standard deviations (SDs) of the naïve rats or a value lower than the mean – 2 SDs of the naïve rats were considered to have a deficit. Because 95% of the observations fall within the mean ± 2 SDs range, there is a chance of less than 5% (corresponding to a p-value of 0.05) to identify TBI animals without a deficit as TBI animals with a deficit, that is, making a type I error (including false-positives). These analyses were performed using GraphPad Prism 6.

For the analysis of longitudinal data (PET, DTI, spontaneous epileptiform activity and seizures over time, MWM learning curves) we made use of linear mixed models in JMP Pro 13, which allowed us to take animals into account for which a data point was missing. Additionally, linear mixed models are more robust against non-normality of data than repeated-measures anaylsis of variances (ANOVAs). For each data set, we fitted linear mixed models with Group (naïve/sham/CCI), Time (two time-points), and the interaction between Group and Time as fixed effects and either Subject alone (random intercept model, smaller model) or both Subject and Subject*Time as random effects (random slope model, larger model). We tested the necessity for the random slope (Subject*Time) with the likelihood ratio test. If the interaction between Group and Time proved to be significant, we performed the appropriate post hoc tests. We did Student's t pairwise comparisons and corrected the p-values for the number of comparisons (Bonferroni correction). Finally, we also performed forward stepwise regression analysis in JMP Pro 13 with p-value threshold as stopping rule (prob to enter: 0.25, prob to leave: 0.1). Statistical significance was set at $p \leq 0.05$.

Results

Subacute brain inflammation after CCI-injury

Analysis of the PET scans revealed significantly higher SUVs of TSPO ligand [^{18}F]PBR111 in the lesion (left parietal cortex, mean ± SEM volume: 16.4 ± 1.8mm^3), perilesional cortex, and ipsilesional hippocampus of CCI-injured rats compared with sham-operated rats, which decreased over time (Fig. 2 A,B; Supplementary Fig. 1; see online supplementary material at http://www.liebertpub.com). For each of these brain regions, a significant interaction between Group and Time ($p \leq 0.01$) was noted. Post hoc testing revealed a significantly higher SUV for each of these brain regions in CCI-injured rats compared with shams at 7 days post-injury (lesion and ipsilesional hippocampus: $p \leq 0.0001$, perilesional cortex: $p \leq 0.001$). At 21 days post-injury, there was still a significantly higher SUV in the ipsilesional hippocampus of CCI-injured rats versus shams ($p \leq 0.01$), but the difference was smaller than at 7 days post-injury. In the other brain regions, no significant difference was present anymore at 21 days post-injury. There was a significant decrease in SUVs between 7 days and 21 days post-injury in the lesion, perilesional cortex, and ipsilesional hippocampus of CCI-injured rats ($p \leq 0.0001$), whereas in sham-operated rats there was no change in SUV over time. No significant difference in SUVs between CCI-injured and sham-operated rats was observed at any time-point in contralateral brain regions.

Radiometabolite analysis revealed no significant difference in metabolization of the radiotracer between sham-operated and CCI-injured rats (respectively, 14.4 ± 0.9% and 15.6 ± 1.0% intact tracer in plasma at 50 min post-injection).

Histology confirms gliosis in the subacute phase following CCI-injury

The area fraction of CD11b-positive staining was significantly higher in the perilesional cortex and ipsilesional hippocampus of CCI-injured rats compared with both naïve and sham-operated rats at 7 days post-injury ($p \leq 0.01$). There was no significant difference in the area fraction of CD11b-positive staining in the contralesional cortex and hippocampus of the three groups (Supplementary Fig. 2; see online supplementary material at http://www.liebertpub.com).

The area fraction of GFAP-positive staining was significantly higher in the perilesional cortex of CCI-injured rats compared with both naïve and sham-operated rats at 7 days post-injury (respectively $p \leq 0.05$ and $p \leq 0.01$). The area fraction of GFAP-positive staining was also significantly higher in the ipsilesional hippocampus of CCI-injured rats compared with naïve rats ($p \leq 0.05$). There was no significant difference in the percent area of GFAP-positive staining in the contralesional cortex and hippocampus of the three groups (Supplementary Fig. 3; see online supplementary material at http://www.liebertpub.com).

Qualitative comparison of TSPO *in vitro* autoradiographs, CD11b- and GFAP-stained tissue sections from the same CCI-injured animals shows that the CD11b staining pattern matches the TSPO binding pattern more closely than the GFAP staining pattern does at this time-point (Supplementary Fig. 4; see online supplementary material at http://www.liebertpub.com).

Subacute microstructural alterations after CCI-injury

After CCI-injury, FA was decreased in the lesion, perilesional cortex, and ipsilesional hippocampus at 4 days post-injury compared with shams. At 18 days post-injury, FA was significantly decreased in the lesion, but not in any other brain region (Fig. 3A,B; Supplementary Fig. 5A; see online supplementary material at http://www.liebertpub.com). Linear mixed model analysis showed a significant effect of Group on FA in the lesion ($p \leq 0.0001$), whereas in the perilesional cortex and ipsilesional hippocampus, a significant interaction between Group and Time (respectively $p \leq 0.0001$ and $p \leq 0.05$) was present. Post hoc analysis showed a significant difference between sham-operated and CCI-injured rats at 4 days post-injury in perilesional cortex ($p \leq 0.0001$) and ipsilesional hippocampus ($p \leq 0.05$). In addition, there was a significant difference between 4 and 18 days in CCI-injured rats in the perilesional cortex ($p \leq 0.0001$) and ipsilesional hippocampus ($p \leq 0.05$). Finally, there was also an effect of time on FA in contralateral cortex ($p \leq 0.05$) (Supplementary Fig. 5A). No significant

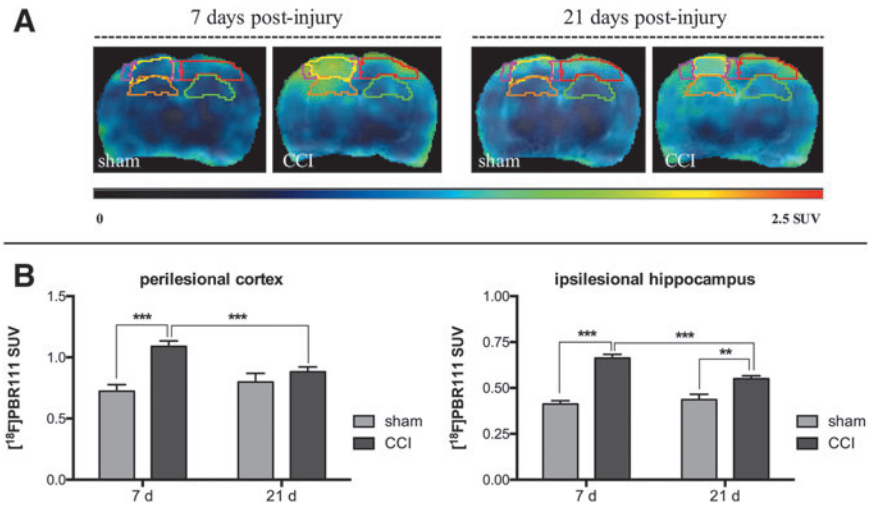

FIG. 2. Subacute PET imaging with [^{18}F]PBR111 in CCI-injured rats. **(A)** Representative positron emission tomography (PET) images of sham-operated and controlled cortical impact (CCI)-injured rats at 7 and 21 days post-injury. Yellow: lesion, pink: perilesional cortex, red: contralateral cortex, orange: ipsilesional hippocampus, green: contralesional hippocampus. **(B)** [^{18}F]PBR111 standardized uptake values (SUVs) in perilesional cortex and ipsilesional hippocampus of sham-operated ($n=5$) and CCI-injured rats ($n=17$). The [^{18}F]PBR111 SUV was significantly higher in both perilesional cortex and ipsilesional hippocampus of CCI-injured rats compared with shams at 7 days post-injury as well as in ipsilesional hippocampus at 21 days post-injury. The SUVs decreased in both regions over time in CCI-injured rats. Mean ± standard error of the mean (SEM) is given. $^{**}p \le 0.01$, $^{***}p \le 0.001$. Color image is available online.

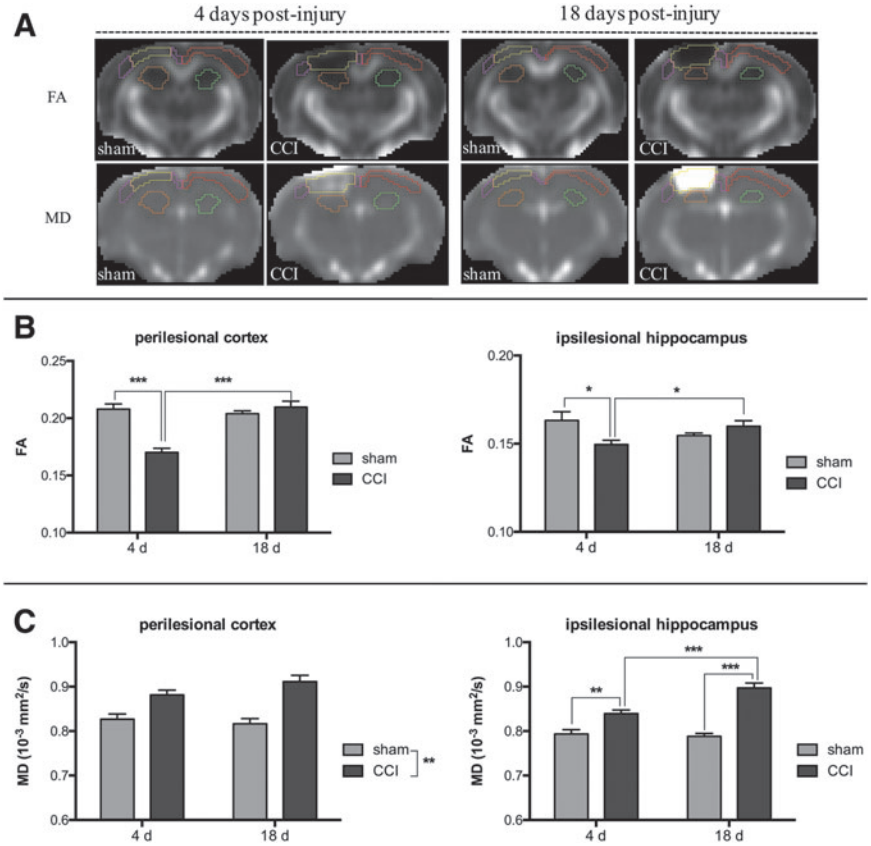

FIG. 3. Subacute diffusion tensor imaging in CCI-injured rats. **(A)** Representative fractional anisotropy (FA) and mean diffusivity (MD) maps of sham-operated and controlled cortical impact (CCI)-injured rats at 4 and 18 days post-injury. Yellow: lesion, pink: perilesional cortex, red: contralateral cortex, orange: ipsilesional hippocampus, green: contralesional hippocampus. **(B)** FA in perilesional cortex and ipsilesional hippocampus of sham-operated ($n=5$) and CCI-injured rats ($n=17$). FA was significantly lower in the perilesional cortex and ipsilesional hippocampus of CCI-injured rats compared with shams at 4 days post-injury. FA increased significantly over time in both perilesional cortex and ipsilesional hippocampus of CCI-injured rats. **(C)** MD in perilesional cortex and ipsilesional hippocampus of sham-operated ($n=5$) and CCI-injured rats ($n=17$). MD was significantly higher in the perilesional cortex and ipsilesional hippocampus of CCI-injured rats compared with shams at both 4 and 18 days post-injury. MD increased significantly over time in the ipsilesional hippocampus of CCI-injured rats. Mean ± standard error of the mean (SEM) is given. $^{*}p \le 0.05$, $^{**}p \le 0.01$, $^{***}p \le 0.001$. Color image is available online.

effect of Group or Time on FA was noted in the contralesional hippocampus (Supplementary Fig. 5A).

After CCI-injury MD, AD, and RD were increased in the lesion, perilesional cortex, and ipsilesional hippocampus versus shams, which was more pronounced at the later time-point (Fig. 3A,C; Supplementary Fig. 5B). Analysis with linear mixed models revealed a significant effect of Group on MD, AD, and RD in the perilesional cortex (MD: $p \leq 0.01$, AD: $p \leq 0.05$, RD: $p \leq 0.001$). For all of these parameters, there was a significant interaction between Group and Time for lesion ($p \leq 0.0001$) and ipsilesional hippocampus ($p \leq 0.01$). Post hoc analysis showed a significant increase in MD, AD, and RD in the lesion of CCI-injured rats at 4 days ($p \leq 0.01$) and 18 days post-injury ($p \leq 0.0001$) versus shams, as well as a significant effect of time in CCI-injured rats ($p \leq 0.0001$). There was a significant increase in MD, AD, and RD in the ipsilesional hippocampus of CCI-injured rats compared with sham-operated rats at 4 days (MD, RD: $p \leq 0.01$, AD: $p \leq 0.05$) and 18 days post-injury (MD, AD, RD: $p \leq 0.001$). All of these parameters significantly differed between 4 and 18 days in CCI-injured rats ($p \leq 0.0001$). There was also a significant interaction between Group and Time effects on MD in contralesional cortex and hippocampus (both $p \leq 0.05$). Post hoc analysis showed that there was (1) a weak trend toward significance for a difference in MD in contralesional cortex at 4 days between CCI-injured rats and sham-operated rats ($p = 0.09$) and (2) a significant difference in MD in contralesional hippocampus between 4 and 18 days post-injury in CCI-injured rats ($p \leq 0.0001$) (Supplementary Fig. 5B). There was also a significant effect of Time on RD in the contralesional hippocampus (increase over time, $p \leq 0.05$). Finally, there was no significant effect of Group or Time on AD or RD in the contralateral cortex and AD in contralesional hippocampus.

TSPO binding correlates with DTI parameters in the lesion of CCI-injured rats

We investigated whether there was a relationship between [^{18}F]PBR111 SUVs and DTI parameters (FA, MD, AD, and RD) in the different ROIs in CCI-injured rats. A positive correlation was observed between [^{18}F]PBR111 SUV and FA in the lesion at 4 days ($p \leq 0.05$, $r = 0.48$) and 18 days post-injury ($p \leq 0.05$, $r = 0.52$), as well as negative correlations between [^{18}F]PBR111 SUV and MD, AD and RD at 4 days (MD: $p \leq 0.01$, $r = -0.60$; AD: $p \leq 0.01$, $r = -0.59$; RD: $p \leq 0.01$, $r = -0.60$) and 18 days post-injury (MD: $p \leq 0.01$, $r = -0.62$; AD: $p \leq 0.01$, $r = -0.63$; RD: $p \leq 0.01$, $r = -0.62$) (Supplementary Fig. 6; see online supplementary material at http://www.liebertpub.com). No significant correlations were observed for the other investigated brain regions.

Chronic deficits after CCI-injury

Disinhibition

Cohort 1. The percent distance moved in the center of the open field arena was significantly higher in CCI-injured rats than in naïve rats ($p \leq 0.05$) (Fig. 4A). There was no significant difference between the three groups in any of the other investigated parameters, including total distance moved and mean velocity.

Cohort 2. To corroborate this observation, we performed the same test in a separate cohort of animals at approximately 2 months post-injury (naïve: $n = 9$, sham: $n = 10$, CCI: $n = 10$) and we observed a significantly increased percent distance moved in the center ($p \leq 0.05$), a significantly increased number of entries into the center ($p \leq 0.05$), and a trend for an increased percent time spent in center ($p = 0.06$) in CCI-injured rats compared with naïve animals

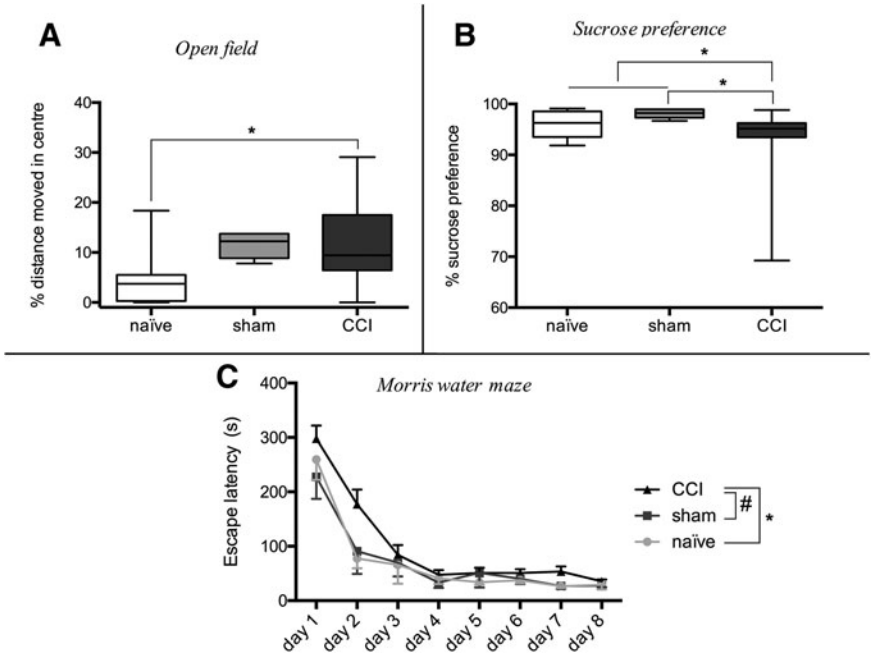

FIG. 4. Chronic behavioral deficits in CCI-injured rats. **(A)** Open field test. Controlled cortical impact (CCI) rats showed a significantly higher percent distance moved in the center of the open field arena compared with naïve rats (naïve: $n = 8$, sham: $n = 5$, CCI: $n = 18$). **(B)** Sucrose preference test. CCI rats had a significantly lower percent sucrose preference compared with shams and all controls (naïve: $n = 8$, sham: $n = 5$, CCI: $n = 18$). **(C)** Morris water maze (MWM) test. CCI rats had a significantly longer escape latency than naïve rats as well as a trend for a longer latency compared with shams during acquisition of the MWM test (naïve: $n = 8$, sham: $n = 5$, CCI: $n = 16$). Data are presented as boxplots (A,B) or mean ± standard error of the mean (SEM) is given (C). #$p \leq 0.1$, *$p \leq 0.05$.

(data not shown). The total distance moved (in center + periphery) and mean velocity were not different between the three groups.

Anhedonia

Cohort 1. CCI-injured rats had a significantly lower percent sucrose preference compared with sham-operated rats and all controls (sham-operated + naïve rats) ($p \leq 0.05$) (Fig. 4B).

Spontaneous epileptiform activity and seizures

Cohort 1. At 6 months post-injury no difference was observed between naïve, sham-operated, and CCI-injured animals regarding number of EDs per day, number of seizures per day (all electrographic), or duration of all epileptiform activity per day (data not shown). At this time-point no behavioral seizures were observed.

Cohort 1. At 9 months post-injury behavioral seizures were observed. CCI-injured rats showed a trend for an increased frequency of behavioral seizures compared with naïve animals ($p = 0.06$) (Fig. 5C). No difference was observed between the three groups for any other investigated parameter. Most behavioral seizures that were recorded were S1 seizures, typically displaying a spike-wave pattern (Fig. 5A-1) or high-voltage rhythmic spike pattern (Fig. 5A-2), and manifested by a behavioral arrest (absence-like seizures). A few other types of behavioral seizures were recorded. One CCI-injured rat experienced two S3 seizures (Fig. 5A-3) and one S2 seizure during the one-week monitoring period at 9 months post-injury. Another CCI-injured rat experienced one S2 seizure. A sham-operated rat experienced one S4 seizure during the one-week monitoring period. Taken together, there was only one rat with spontaneous recurrent convulsive seizures at 9 months post-injury. Hence, the incidence of post-traumatic epilepsy was 14% (1/7 vEEG monitored CCI-injured rats) in our study.

In addition, we investigated the evolution of spontaneous epileptiform activity and seizures over time. There were significantly more EDs and seizures per day at 9 months post-injury than at 6 months post-injury in both sham-operated and CCI-injured rats ($p \leq 0.05$) (Fig. 5B). Finally, the duration of all epileptiform activity per day was significantly higher at 9 months versus 6 months post-injury in these groups ($p \leq 0.01$). There was no difference between sham-operated and CCI-injured rats. No naïve rats were longitudinally subjected to vEEG monitoring for the investigation of spontaneous epileptiform activity.

Seizure susceptibility

Cohort 1. At 6 months post-injury, CCI-injured rats showed a non-significant trend for a shorter latency to the first spike compared with naïve animals ($p = 0.08$) (Fig. 5D). A very weak trend was observed for an increased number of EDs in TBI rats compared with naïve rats ($p = 0.10$) (Fig. 5E). There was no difference between the three groups for latency to first ED and seizure, and number of spikes and seizures. At this time-point only 23% (5/22) of all rats experienced a convulsive seizure (usually S5) after injection with 25 mg/kg PTZ with no difference between the three groups (χ^2, $p > 0.05$) (data not shown).

Cohort 1. At 9 months post-injury 60% (9/15) of all rats developed a convulsive seizure (usually S5) after administration of 30 mg/kg PTZ: 25% (1/4) naïve rats, 50% (2/4) sham-operated rats, and 86% (6/7) CCI-injured rats (χ^2, $p \leq 0.05$). When comparing the three groups, we observed a trend for an increased number of convulsive seizures ($p = 0.08$) and a significantly increased total duration of convulsive seizures in CCI-injured rats compared with naïve animals ($p \leq 0.05$) (Fig. 5I). We pooled the two control groups (naïve and sham-operated animals) to be able to perform statistics regarding the latency to the first convulsive seizure and observed a significantly shorter latency to first convulsive seizure in CCI-injured rats versus controls ($p \leq 0.05$) (Fig. 5H). In addition, we observed a trend for a decreased number of EDs in CCI-injured rats compared with naïve rats ($p = 0.07$) (Fig. 5G). Upon further investigation, we observed a strong relationship between number of EDs and latency to first convulsive seizure in the rats ($r = 0.88$, $p \leq 0.1$) (data not shown). Hence, a decreased latency to the first convulsive seizure coincides with a decreased number of EDs. We observed no difference between the three groups for any other investigated parameter (latency to first spike and ED, number of spikes and EDs) (Fig. 5F).

One CCI-injured animal went into *status epilepticus* (six convulsive seizures in one h) after administration of 30 mg/kg PTZ. The rat died shortly after the test, before diazepam could be administered to stop the *status epilepticus*. This was also the only CCI-injured rat that experienced multiple spontaneous convulsive seizures during the one-week monitoring period at 9 months post-injury.

Cohort 2. Additionally, we performed a PTZ test in a separate cohort of animals at approximately 6 months post-injury, but without EEG monitoring. Behavioral monitoring of animals indicated that 11% (1/9) naïve rats, 40% (4/10) sham-operated rats, and 78% (7/9) CCI-injured rats developed a generalized tonic-clonic (S5) seizure following administration of 30 mg/kg PTZ (χ^2, $p \leq 0.01$).

Impaired visuospatial learning

Cohort 1. Analysis with linear mixed models showed a significant effect of both Group ($p \leq 0.05$) and Time (= trial block) ($p \leq 0.0001$) on both escape latency and path length to the platform. There was no significant interaction between Group and Time. Post hoc analysis revealed that CCI-injured animals had a significantly longer escape latency than naïve animals ($p \leq 0.05$) and a weak trend for a longer latency compared with sham-operated rats ($p = 0.09$) (Fig. 4C). The difference was seen to be greatest at the second day of training. CCI-injured animals also showed a trend for an increased path length compared with naïve rats ($p = 0.06$) (data not shown). There was no difference in the swimming speed between the three groups.

Although a numerically lower percent time spent in the target quadrant during the probe trial was observed in CCI-injured animals versus the controls, no significant difference between the three groups was noted. There was a trend for a lower frequency of platform crossings in CCI-injured rats compared with sham-operated rats ($p = 0.08$) (data not shown).

Correlation between subacute TSPO binding, microstructural changes, lesion volume, and chronic deficits in CCI-injured rats

First of all, we investigated if there was a correlation between (1) subacute TSPO expression ([^{18}F]PBR111 SUV) in perilesional cortex, ipsilesional hippocampus, contralesional cortex, and contralesional hippocampus of CCI-injured rats, (2) DTI metrics in these brain regions, and (3) lesion volume on the one hand and chronic behavioral deficits on the other hand (i.e., parameters that were significantly different in CCI-injured rats compared with controls or showed a trend toward significance). In addition, we investigated whether the evolution in TSPO expression, DTI metrics, and lesion volume (i.e., the

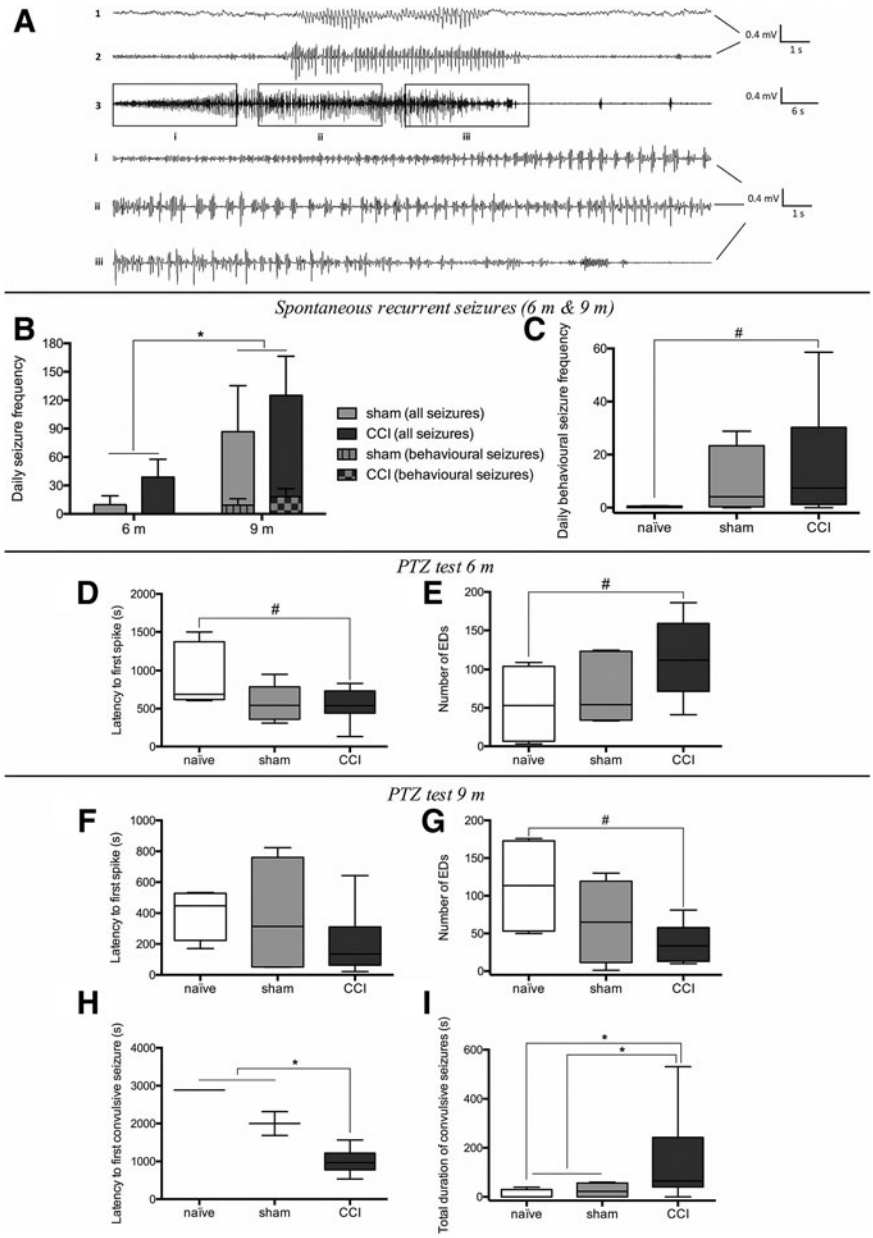

FIG. 5. Spontaneous recurrent seizures (SRS) and seizure susceptibility in controlled cortical impact (CCI)-injured rats. **(A–C)** SRS. (A) Representative examples of SRS that were observed during video-electroencephalogram (vEEG) monitoring. 1: spike-wave discharge (SWD), 2: high-voltage rhythmic spike (HVRS) discharge, 3: convulsive S3 seizure. i: beginning, ii: middle, and iii: end of the convulsive seizure. (B) Both sham-operated and CCI-injured rats had a significantly higher spontaneous seizure frequency at 9 months versus 6 months post-injury (6 months: $n=4$ sham, $n=17$ CCI; 9 months: $n=4$ sham, $n=7$ CCI) (C) There was a trend for a higher daily frequency of behavioral SRS in CCI-injured rats compared with naïve rats (naïve: $n=4$, sham: $n=4$, CCI: $n=7$). **(D,E)** Pentylenetetrazole (PTZ) seizure susceptibility test at 6 months post-injury. (D) CCI-injured rats showed a trend for a shorter latency to first spike following 25 mg/kg PTZ injection compared with naïve rats (naïve: $n=5$, sham: $n=5$, CCI: $n=13$). (E) CCI-injured rats showed a trend for a higher number of epileptiform discharges (EDs) (naïve: $n=4$, sham: $n=5$, CCI: $n=13$). **(F–I)** PTZ test at 9 months post-injury. (F) There was no difference in latency to first spike following 30 mg/kg PTZ injection between any of the groups (naïve: $n=4$, sham: $n=4$, CCI: $n=7$). (G) CCI-injured rats showed a trend for a lower number of epileptiform discharges (EDs) (naïve: $n=4$, sham: $n=4$, CCI: $n=6$). (H) CCI rats had a significantly shorter latency to first convulsive seizure versus all controls (naïve: $n=1$, sham: $n=2$, CCI: $n=6$). (I) CCI rats had a significantly higher total duration of convulsive seizures than naïve rats and all controls following 30 mg/kg PTZ injection (naïve: $n=4$, sham: $n=4$, CCI: $n=6$). Data are presented as boxplots (C–I) or mean ± standard error of the mean (SEM) is given (B). $\#p \leq 0.1$, $*p \leq 0.05$.

percent change in SUV, FA, MD, AD, RD, and lesion volume over time) correlated with the chronic functional outcome.

Several correlations were observed between individual TSPO PET and DTI parameters on the one hand and chronic deficits on the other hand (ipsilesional brain regions: Fig. 6 and Fig. 7; contralesional brain regions: Supplementary Fig. 7 and Supplementary Fig. 8; see online supplementary material at http://www.liebertpub.com). Correlations that were significant are summarized in Table 1 (TSPO PET in ipsilesional brain regions), Table 2 (DTI in ipsilesional brain regions), Supplementary Table 1 (TSPO PET in contralesional

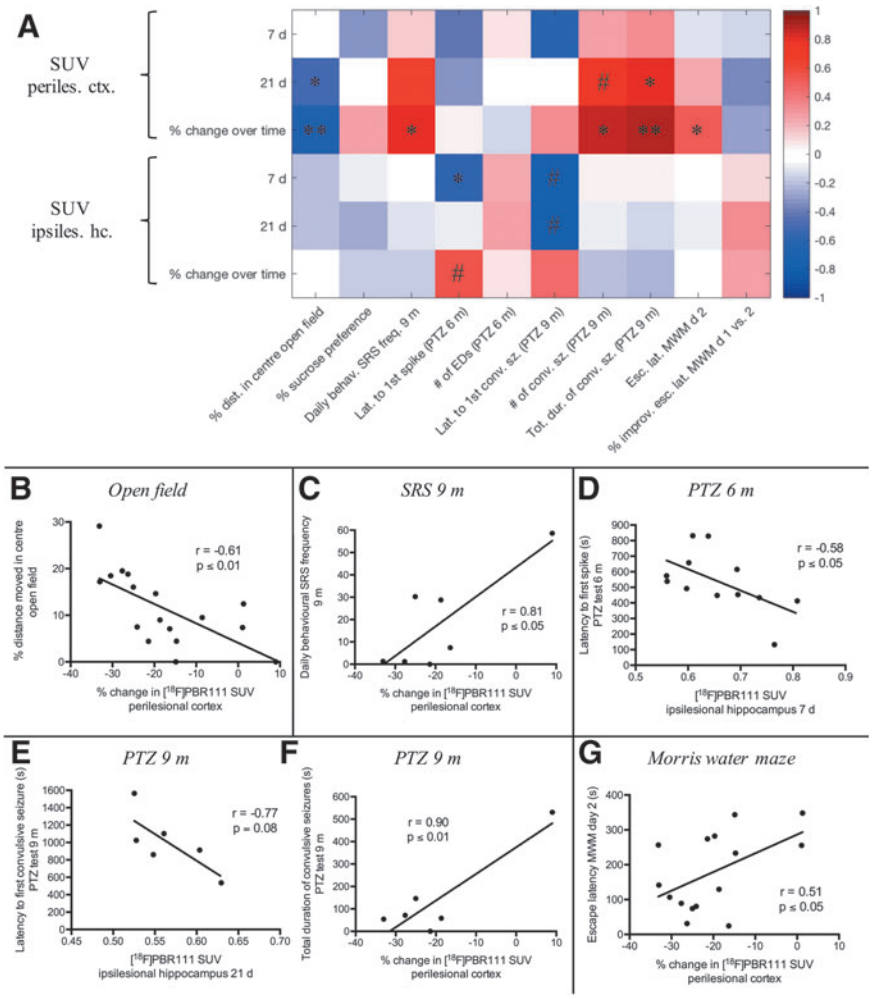

FIG. 6. Correlation between subacute brain inflammation in ipsilesional brain regions and long-term functional outcome in controlled cortical impact (CCI)-injured rats. **(A)** Color-coded correlation matrix between translocator protein (TSPO) positron emission tomography (PET) measurements and functional deficits (red = positive Pearson's r, blue = negative Pearson's r). Periles. ctx. = perilesional cortex, ipsiles. hc. = ipsilesional hippocampus, dist. = distance, behav. = behavioral, freq. = frequency, lat. = latency, # = number, conv. = convulsive, sz. = seizure(s), tot. = total, dur. = duration, esc. = escape, improv. = improvement. **(B)** There was a negative correlation between the percent change in [^{18}F]PBR111 standardized uptake value (SUV) in perilesional cortex over time and the percent distance moved in the center of the open field. **(C)** A positive correlation was observed between the percent change in SUV in perilesional cortex over time and the daily behavioral seizure frequency at 9 months post-injury. **(D)** A negative correlation was observed between the SUV in ipsilesional hippocampus at 7 days post-injury and the latency to the first spike following pentylenetetrazole (PTZ) administration at 6 months post-injury. **(E)** There was a trend for a negative correlation between the SUV in ipsilesional hippocampus at 21 days post-injury and the latency to the first convulsive seizure following PTZ administration at 9 months post-injury. **(F)** There was a positive correlation between the percent change in [^{18}F]PBR111 SUV in perilesional cortex over time and the total duration of convulsive seizures during the PTZ seizure susceptibility assay at 9 months post-injury. **(G)** A positive correlation was seen between the percent change in SUV in perilesional cortex over time and the escape latency on day 2 of the Morris water maze (MWM) test. #$p \leq 0.1$, *$p \leq 0.05$, **$p \leq 0.01$. Color image is available online.

brain regions), and Supplementary Table 2 (DTI in contralesional brain regions). Most importantly, both TSPO PET and DTI parameters correlated with disinhibition in the open field, spontaneous behavioral seizure frequency at 9 months post-injury, increased seizure susceptibility, and MWM performance.

The lesion volume at 4 and 18 days post-injury correlated with the number of EDs during the PTZ test at 6 months post-injury (respectively r = 0.67, $p \leq 0.05$ and r = 0.68, $p \leq 0.05$) (Supplementary Fig. 9A,B; see online supplementary material at http://www.liebertpub.com). There were no significant correlations with any other chronic deficit.

ROC curve analysis

ROC curves were plotted for those *in vivo* imaging parameters that correlated significantly with chronic deficits in the Pearson correlation analysis (see Tables 1, 2; Supplementary Tables 1, 2). ROC curves were only plotted if there was a sufficient number of animals ($n \geq 5$) in each group (i.e., CCI-injured animals with deficit and CCI-injured animals without deficit). This excluded ROC curves with behavioral seizure frequency at 9 months and seizure susceptibility at 6 and 9 months post-injury as outcome. In total, 11 ROC curves were plotted: six for ipsilesional measurements (Fig. 8)

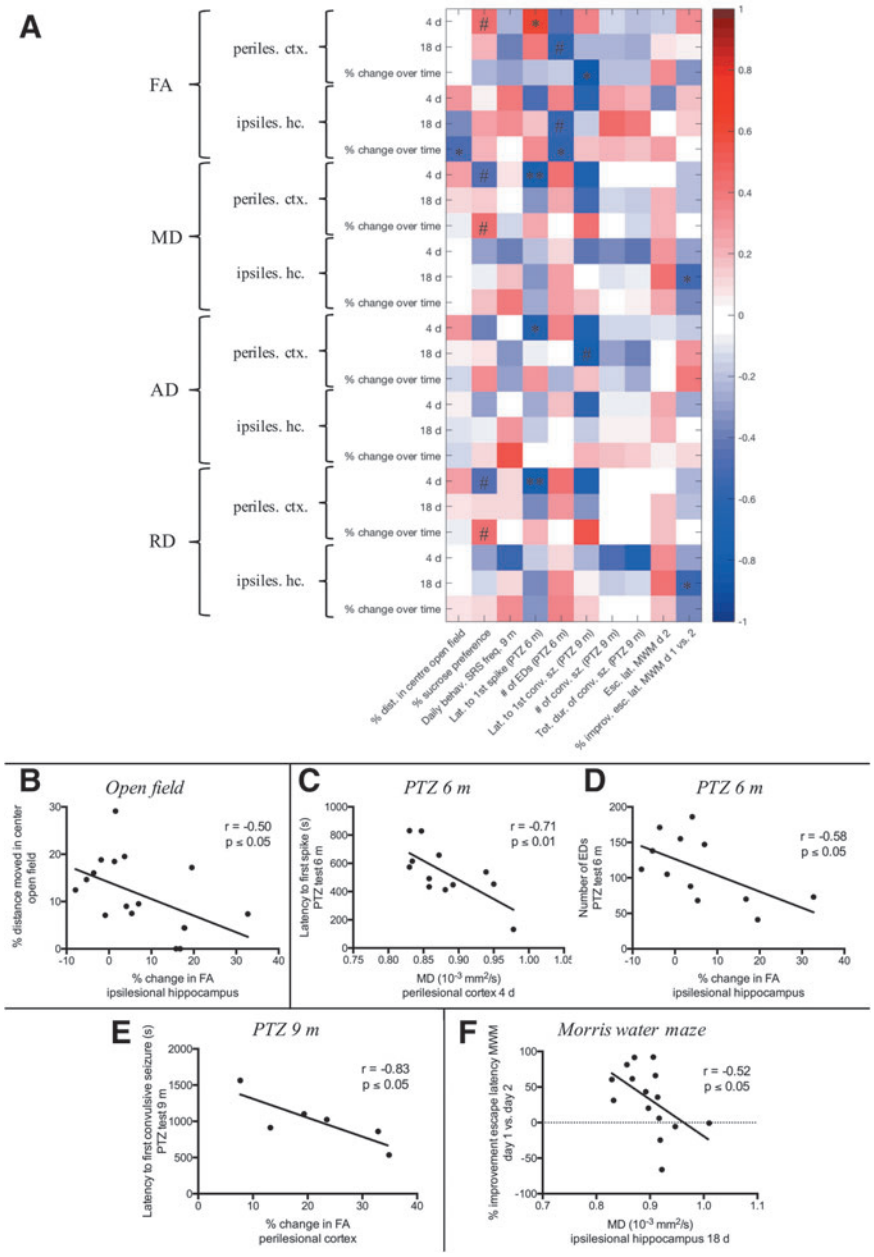

FIG. 7. Correlation between subacute microstructural changes in ipsilesional brain regions and long-term functional outcome in controlled cortical impact (CCI)-injured rats. **(A)** Color-coded correlation matrix between diffusion tensor imaging (DTI) measurements and functional deficits (red = positive Pearson's r, blue = negative Pearson's r). Periles. ctx. = perilesional cortex, ipsiles. hc. = ipsilesional hippocampus, dist. = distance, behav. = behavioral, freq. = frequency, lat. = latency, # = number, conv. = convulsive, sz. = seizure(s), tot. = total, dur. = duration, esc. = escape, improv. = improvement. **(B)** There was a negative correlation between the percent change in fractional anisotropy (FA) in ipsilesional hippocampus over time and the percent distance moved in the center of the open field. **(C)** A negative correlation was seen between mean diffusivity (MD) in perilesional cortex at 4 days post-injury and the latency to the first spike following PTZ administration at 6 months post-injury. **(D)** A negative correlation was found between the percent change in FA in ipsilesional hippocampus over time and the total number of epileptiform discharges (EDs) during the PTZ seizure susceptibility assay at 6 months post-injury. **(E)** There was a negative correlation between the relative change in FA in perilesional cortex and the latency to first convulsive seizure following PTZ administration at 9 months post-injury. **(F)** A negative correlation was observed between MD in ipsilesional hippocampus at 18 days post-injury and the percent improvement in escape latency between day 1 and day 2 of the Morris water maze (MWM) test. #$p \leq 0.1$, *$p \leq 0.05$, **$p \leq 0.01$. Color image is available online.

and five for contralesional measurements (Supplementary Fig. 10; see online supplementary material at http://www.liebertpub.com).

Whereas the [^{18}F]PBR111 SUV in perilesional cortex at 21 days post-injury showed relatively good sensitivity and specificity in distinguishing between CCI-injured rats with and without disinhibition in the open field (area under the ROC curve [AUC] = 0.80, $p = 0.06$), the relative change over time in [^{18}F]PBR111 SUV in this brain region had a much higher sensitivity and specificity in distinguishing between CCI-injured rats with and without disinhibition (AUC = 1.00, $p \leq 0.01$) (Fig.8 A,B). The relative change over time in FA in ipsilesional

Table 1. Significant Correlations between Subacute TSPO PET Measurements in the Ipsilesional Hemisphere and Chronic Functional Deficits

Chronic deficit	*TSPO PET parameter*	*Pearson's r*	P-*value*
% distance moved in center open field	SUV 21 d perilesional cortex	–0.52	$p \leq 0.05$
	% change SUV over time perilesional cortex	–0.66	$p \leq 0.01$
Daily behavioral seizure frequency 9 m	% change SUV over time perilesional cortex	0.81	$p \leq 0.05$
Latency to first spike (PTZ test 6 m)	SUV 7 d ipsilesional hippocampus	–0.58	$p \leq 0.05$
Number of convulsive seizures (PTZ test 9 m)	% change SUV over time perilesional cortex	0.85	$p \leq 0.05$
Total duration of convulsive seizures (PTZ test 9 m)	SUV 21 d perilesional cortex	0.81	$p \leq 0.05$
	% change SUV over time perilesional cortex	0.90	$p \leq 0.01$
Escape latency MWM day 2	% change SUV over time perilesional cortex	0.51	$p \leq 0.05$

MWM, Morris water maze; PET, positron emission tomography; PTZ, pentylenetetrazole; SUV, standardized uptake values; TSPO, translocator protein.

hippocampus showed no good sensitivity and specificity in distinguishing between CCI-injured rats with and without disinhibition (AUC = 0.57, $p > 0.05$) (Fig. 8D). The [^{18}F]PBR111 SUV in contralesional cortex at 21 days post-injury was also not able to distinguish between CCI-injured rats with and without disinhibition (AUC = 0.75, $p > 0.05$). However, the [^{18}F]PBR111 SUV in contralesional hippocampus at this time-point was able to distinguish between the CCI-injured rats with and without disinhibition (AUC = 0.85, $p \leq 0.05$) (Supplementary Fig. 10 A,B). The FA in contralesional cortex at 18 days post-injury showed also very high sensitivity and specificity in distinguishing between rats with and without disinhibition (AUC = 0.92, $p \leq 0.01$), but the other investigated parameters (relative change over time in FA in contralesional cortex: AUC = 0.62, $p > 0.05$; MD in contralesional hippocampus at 18 days post-injury: AUC = 0.60, $p > 0.05$) did not (Supplementary Fig. 10C–E).

The relative change over time in [^{18}F]PBR111 SUV in perilesional cortex showed relatively good sensitivity and specificity in distinguishing between CCI-injured rats with and without a learning deficit in the MWM test (AUC = 0.79, $p = 0.06$) (Fig. 8C). MD and RD in ipsilesional hippocampus at 18 days post-injury showed very good sensitivity and specificity in distinguishing between CCI-injured rats with and without a learning deficit (respectively AUC = 1.00, $p \leq 0.01$ and AUC = 0.96, $p \leq 0.01$) (Fig. 8E,F).

Stepwise regression analysis

Finally, we performed stepwise regression analysis to investigate whether ipsilesional and contralesional TSPO PET data, DTI metrics, or lesion volume alone are sufficient to predict the long-term functional deficits or whether combining TSPO PET, DTI, and lesion volume has an added value. To this end, automated forward stepwise regression analysis was conducted with five different sets of possible predictors, that is, only TSPO PET parameters, only DTI metrics, only lesion volumes, TSPO PET and DTI measurements combined and TSPO PET, DTI and lesion volume assessments combined to build different regression models. The models were then compared to see which of the five models was best at explaining the variability in the data (i.e., the chronic functional deficits). The obtained data are summarized in Table 3 (TSPO PET, DTI, and TSPO PET + DTI models) and Supplementary Table 3 (lesion volume models and comparison between TSPO PET + DTI and TSPO PET + DTI + lesion volume models; see online supplementary material at http://www.liebertpub.com).

Both TSPO PET and DTI parameters alone could explain some of the variability in the percent distance moved in the center of the open field of CCI-injured rats (respectively R^2 adj. = 0.63, $p = 0.001$ and R^2 adj. = 0.54, $p = 0.0043$), but combining these parameters resulted in a better model (R^2 adj. = 1.00, $p < 0.0001$).

Variability in the sucrose preference in CCI-injured rats could be explained by variability in the DTI parameters (R^2 adj. = 0.89, $p < 0.0001$), but could be explained even better by a combination of DTI and TSPO PET parameters (R^2 adj. = 1.00, $p < 0.0001$).

Both TSPO PET and DTI parameters alone can predict the variability in behavioral SRS frequency at 9 months post-injury (respectively R^2 adj. = 0.89, $p = 0.0214$ and R^2 adj. = 0.83, $p = 0.0395$), but a combination of TSPO PET and DTI parameters is even better

Table 2. Significant Correlations between Subacute DTI Measurements in the Ipsilesional Hemisphere and Chronic Functional Deficits

Chronic deficit	*DTI parameter*	*Pearson's r*	P-*value*
% distance moved in centre open field	% change FA over time ipsilesional hippocampus	–0.50	$p \leq 0.05$
Latency to first spike (PTZ test 6 m)	FA 4 d perilesional cortex	0.61	$p \leq 0.05$
	MD 4 d perilesional cortex	–0.71	$p \leq 0.01$
	AD 4 d perilesional cortex	–0.65	$p \leq 0.05$
	RD 4 d perilesional cortex	–0.72	$p \leq 0.01$
Number of EDs (PTZ test 6 m)	% change FA over time ipsilesional hippocampus	–0.58	$p \leq 0.05$
Latency to first convulsive seizure (PTZ test 9 m)	% change FA over time perilesional cortex	–0.83	$p \leq 0.05$
% improvement escape latency MWM day 1 vs. 2	MD 18 d ipsilesional hippocampus	–0.52	$p \leq 0.05$
	RD 18 d ipsilesional hippocampus	–0.54	$p \leq 0.05$

AD, axial diffusivity; DTI, diffusion tensor imaging; ED, epileptiform discharge; FA, fractional anisotropy; MWM, Morris water maze; PTZ, pentylenetetrazole; RD, radial diffusivity.

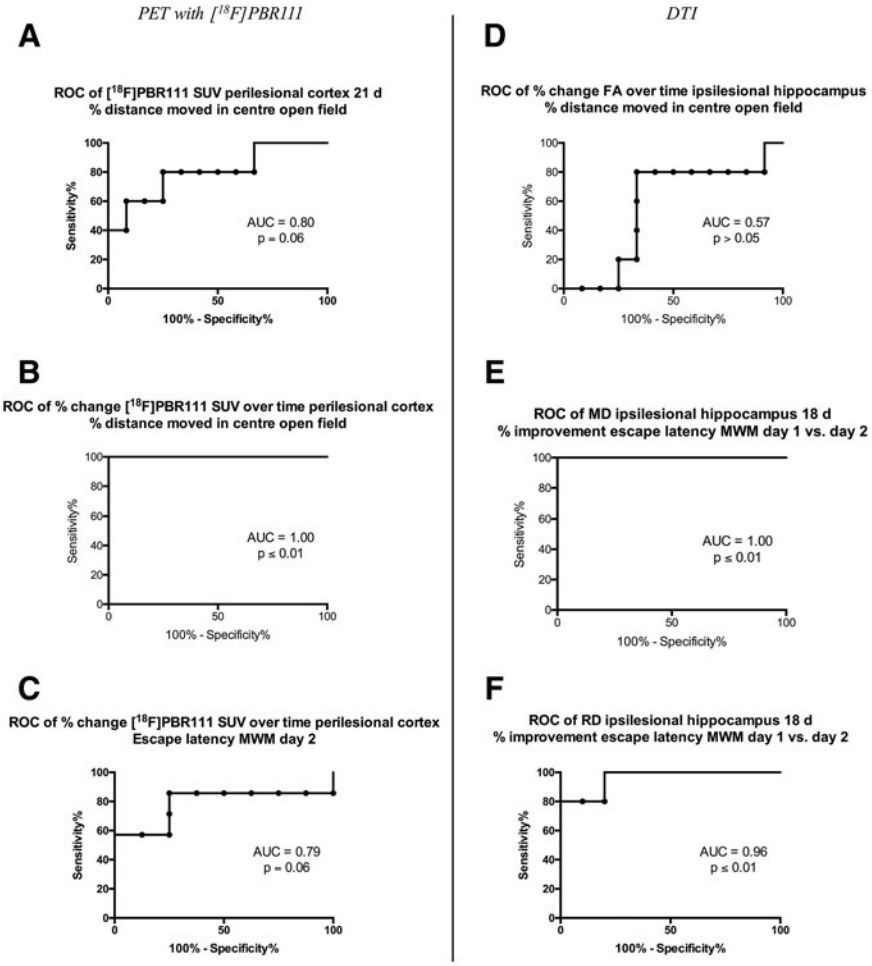

FIG. 8. ROC curve analysis. Some *in vivo* imaging parameters in the ipsilesional hemisphere showed good sensitivity and specificity to distinguish between controlled cortical impact (CCI)-injured rats with and without a particular deficit. **(A)** The [^{18}F]PBR111 standardized uptake value (SUV) in perilesional cortex at 21 days post-injury could fairly well distinguish between traumatic brain injury (TBI) rats with and without disinhibition. **(B)** The percent change in [^{18}F]PBR111 SUV in perilesional cortex over time was able to distinguish between TBI rats with and without disinhibition. **(C)** The percent change in [^{18}F]PBR111 SUV in perilesional cortex over time could fairly well distinguish between TBI rats with and without learning impairment in the Morris water maze (MWM) test. **(D)** The percent change in fractional anisotropy (FA) in ipsilesional hippocampus over time was *not* able to distinguish between TBI rats with and without disinhibition. **(E)** The MD in ipsilesional hippocampus at 18 days post-injury could very well distinguish between TBI rats with and without learning impairment in the MWM test. **(F)** The radial diffusivity (RD) in ipsilesional hippocampus at 18 days post-injury was able to distinguish between TBI rats with and without learning impairment in the MWM test. AUC, area under the ROC curve.

at predicting the variability in this behavioral outcome parameter (R^2 adj. = 1.00, $p = 0.0008$).

DTI parameters are good at predicting the variability in the increased seizure susceptibility at 6 months post-injury (latency to first spike: R^2 adj. = 1.00, $p = 0.0002$; number of EDs: R^2 adj. = 1.00, $p = 0.0003$).

Both TSPO PET and DTI parameters alone as well as the combination of these parameters can predict the variability in the increased seizure susceptibility at 9 months post-injury: latency to first convulsive seizure (TSPO PET: R^2 adj. = 0.91, $p = 0.0122$; DTI: R^2 adj. = 1.00, $p = 0.0017$; TSPO PET + DTI: R^2 adj. = 1.00, $p = 0.0012$), number of convulsive seizures (TSPO PET: R^2 adj. = 0.98, $p = 0.0013$; DTI: R^2 adj. = 1.00, $p = 0.0012$; TSPO PET + DTI: R^2 adj. = 1.00, $p = 0.0015$) and total duration of convulsive seizures (TSPO PET: R^2 adj. = 1.00, $p = 0.0181$; DTI: R^2 adj. = 1.00, $p = 0.0009$; TSPO PET + DTI: R^2 adj. = 1.00, $p = 0.0009$).

Variability in MWM performance can mainly be explained by DTI metrics (escape latency MWM training day 2: R^2 adj. = 1.00, $p = 0.0085$; percent improvement escape latency MWM training day 1 versus day 2: R^2 adj. = 0.95, $p = 0.0002$).

Variability in lesion volume can explain some of the variability in the percent distance moved in the center of the open field of CCI-injured rats (R^2 adj. = 0.36, $p = 0.0285$) as well as in the number of EDs during the seizure susceptibility test at 6 months (R^2 adj. = 0.40, $p = 0.0221$), although not as well as can TSPO PET and DTI parameters. Variability in lesion volume could not explain the variability in any other functional outcome parameter. Adding lesion volume assessments to the TSPO PET + DTI models did not improve any of these prognostic models.

Discussion

The main finding of our study was that both subacute TSPO expression and changes in DTI metrics following CCI-injury correlated with several chronic sequelae. Not only robust changes in TSPO expression and DTI metrics in the ipsilesional brain regions

Table 3. Stepwise Regression Models of Chronic Functional d=Deficits with Ipsi- and Contralesional TSPO PET Measurements Alone, DTI Measurements Alone, and the Combination of TSPO PET and DTI Measurements as Predictors

Functional outcome	*Imaging modality*	R^2	*Adjusted* R^2	P-*value*
Open field				
% distance moved in center	***TSPO PET***	***0.70***	***0.63***	***0.001***
	DTI	***0.62***	***0.54***	***0.0043***
	TSPO PET + DTI	***1.00***	***1.00***	***<0.0001***
Sucrose preference				
% sucrose preference	TSPO PET	0.23	0.12	0.1609
	DTI	***0.94***	***0.89***	***<0.0001***
	TSPO PET + DTI	***1.00***	***1.00***	***<0.0001***
SRS 9 m				
Daily behavioral SRS frequency	***TSPO PET***	***0.95***	***0.89***	***0.0214***
	DTI	***0.92***	***0.83***	***0.0395***
	TSPO PET + DTI	***1.00***	***1.00***	***0.0008***
PTZ 6 m				
Latency to first spike	TSPO PET	0.44	0.32	0.0710
	DTI	***1.00***	***1.00***	***0.0002***
	TSPO PET + DTI	***1.00***	***1.00***	***0.0003***
Number of EDs	TSPO PET	0.32	0.17	0.1757
	DTI	***1.00***	***1.00***	***0.0003***
	TSPO PET + DTI	***1.00***	***1.00***	***0.0031***
PTZ 9 m				
Latency to first convulsive seizure	**TSPO PET**	**0.95**	**0.91**	**0.0122**
	DTI	***1.00***	***1.00***	***0.0017***
	TSPO PET + DTI	***1.00***	***1.00***	***0.0012***
Number of convulsive seizures	***TSPO PET***	***0.99***	***0.98***	***0.0013***
	DTI	***1.00***	***1.00***	***0.0012***
	TSPO PET + DTI	***1.00***	***1.00***	***0.0015***
Total duration of convulsive seizures	***TSPO PET***	***1.00***	***1.00***	***0.0181***
	DTI	***1.00***	***1.00***	***0.0009***
	TSPO PET + DTI	***1.00***	***1.00***	***0.0009***
MWM				
Escape latency day 2	TSPO PET	0.26	0.20	0.0527
	DTI	***1.00***	***1.00***	***0.0085***
	TSPO PET + DTI	***1.00***	***1.00***	***0.0001***
% improvement escape latency day 1 vs. day 2	TSPO PET	0.29	0.17	0.1299
	DTI	***0.98***	***0.95***	***0.0002***
	TSPO PET + DTI	***0.75***	***0.65***	***0.0046***

Significant models for each functional outcome parameter are indicated in bold and italic.

DTI, diffusion tensor imaging; ED, epileptiform discharge; MWM, Morris water maze; PET, positron emission tomography; PTZ, pentylenetetrazole; SRS, spontaneous recurrent seizures; TSPO, translocator protein.

correlated with multiple long-term functional deficits, but also the variability in these parameters in the contralesional brain regions correlated well with these deficits. Importantly, not only the absolute SUV and DTI values at distinct time-points were good correlates of the functional outcome, but also the relative change in TSPO expression and DTI metrics over time. Some of the TSPO PET and DTI measurements showed good sensitivity and specificity in distinguishing TBI rats with and without a particular chronic deficit, making them promising prognostic biomarkers. Depending on the behavioral deficit that is investigated, TSPO PET data or DTI metrics alone, or the combination of the two imaging modalities, can predict the long-term deficit. DTI metrics could predict all the investigated chronic deficits, but TSPO PET could also predict many chronic sequelae, including disinhibition in the open field, spontaneous behavioral seizure frequency, and seizure susceptibility at 9 months post-injury. In several instances, combining TSPO PET and DTI parameters resulted in the best prognostic models for the chronic outcome (open field behavior, sucrose preference, and spontaneous behavioral seizure frequency).

Subacute brain inflammation and microstructural changes after TBI

High TSPO binding of [^{18}F]PBR111 was observed at 7 days post-contusion, which decreased over time. This temporal profile was similar to previously reported binding of other TSPO radioligands in rat contusion models.[16,17,19]

In addition, we performed immunohistochemical stainings against CD11b (expressed by microglia/macrophages) and GFAP (expressed by astrocytes) as well as *in vitro* autoradiography with the TSPO radioligand [^{3}H]PK11195 at 7 days post-injury, when [^{18}F]PBR111 SUVs in CCI-injured animals were the highest. At this time-point we observed high densities of microglia/macrophages and astrocytes in the perilesional cortex and ipsilesional

hippocampus of CCI-injured rats. There was no difference between sham-operated rats and naïve animals, indicating that there is no detectable inflammatory response following craniectomy, at least not at this time-point (Supplementary Figs. 2 and 3). A qualitative comparison of TSPO *in vitro* autoradiographs, CD11b- and GFAP-stained sections of the same animals suggests that at this time-point primarily microglia/macrophages contribute to the TSPO signal (Supplementary Fig. 4). However, a contribution of astrocytes to the TSPO signal is likely. Several studies in TBI models using double stainings came to the same conclusion and pointed to microglia/macrophages as the main cellular sources of the TSPO signal with an additional contribution of astrocytes.[16,17]

PET imaging with second-generation TSPO radiotracers to assess brain inflammation has been applied in clinical studies of several neurological and neuropsychiatric disorders, including TBI, brain infarct, brain tumor, multiple sclerosis, Alzheimer's disease, and schizophrenia. Although promising results have been obtained, several limitations of these radiotracers have been observed. A human gene polymorphism in *TSPO* (rs6971, resulting in Ala147Thr substitution in TSPO) determines the binding affinity of the PET tracers, resulting in a trimodal distribution in binding affinity among subjects.[43,44] There are low-affinity binders, high-affinity binders, and mixed affinity binders. Knowledge of the individual binding status of the patient is therefore required to correctly interpret TSPO PET data. Third-generation TSPO tracers that are less sensitive to this differential binding status are being evaluated. Quantification of TSPO PET results also remains an issue.[45] Many studies using arterial blood sampling for kinetic modeling have reported considerable variability in blood measurements. Moreover, there is no true reference region that can be used for reference tissue modeling.[46]

Decreased anisotropy and increased diffusivity have previously been observed after experimental TBI (reviewed in Hutchinson and colleagues[47]) in line with our findings at 4 days post-TBI. Neuronal cell loss, resulting in a decreased neurite density, axon damage, demyelination, and disorganized gliosis can underlie the decreased anisotropy. The subsequent increase in anisotropy at 18 days post-TBI may be due to neuronal regeneration/reorganization (e.g., axon sprouting), remyelination, and organized gliosis (e.g., glial scarring). Johnstone and colleagues suggested that the increased FA that they observed following FPI in rats was related to structural reorganization, because it coincided with recovery of neuronal responsiveness.[48] Budde and colleagues, however, attributed increased FA following CCI-injury in rats to coherent organization of reactive astrocytes (i.e., glial scarring) and not to regeneration/structural reorganization of axons.[49] We cannot conclude which process attributed to the increased FA in our study. Although the increase in FA in perilesional cortex over time did not coincide with an increase in TSPO expression, it cannot be excluded that glial scarring did not contribute to the increased FA. The decrease in TSPO over time may primarily reflect a decrease in microglial density/activity, rather than a decrease in reactive astrocytes, which are the main contributors to the glial scar. The increased diffusivity may be explained by vasogenic edema, neuronal cell death, and gliosis (e.g., amoeboid microglia).[47] A worsening of the diffusivity over time may reflect secondary injury.[50]

Further, we observed a correlation between high TSPO binding in the lesion on the one hand and high anisotropy (FA) and low diffusivity (MD, AD, and RD) in the lesion on the other hand, supporting the hypothesis that gliosis contributed to the observed changes in DTI parameters. A high infiltration of TSPO-positive immune cells (i.e., high cellularity) into the lesioned area that is otherwise only filled with cell debris and extracellular fluid can explain lower diffusivity and higher anisotropy.

TBI results in tissue loss, which is most prominent and acute at the lesion site. Also in perilesional areas there is damage and ultimately loss of neurons, which is part of the secondary, delayed injury. Damage to neurons elicits a complex neuroinflammatory response, involving many immune-competent cells. Part of their job is to remove the cellular debris, which is caused by the loss of neurons. Hence, one imaging signature of tissue loss is an increase in immune cells that clear the debris, which may be detected by TSPO PET. Tissue loss can also cause hypometabolism, which can be measured with fluorodeoxyglucose (FDG) PET. Increased inflammation and hypometabolism have been shown to occur in parallel after TBI.[17] Complete loss of neurons, damage to cell membranes, and axonal injury can cause an increased mean diffusivity and decreased anisotropy, as we have observed acutely in our study. Removal of cell debris by immune cells can increase the diffusivity even further. Delayed loss of neurons in perilesional areas (secondary injury) can also cause a further increase in diffusivity. Indeed, we have observed a worsening of the diffusivity over time in our study. Hence, tissue loss also has several imaging signatures that can be measured with DTI.

Chronic sequelae of TBI

CCI-injured rats exhibited several chronic deficits compared with naïve and/or sham-operated animals. Whereas naïve and sham-operated rats did not differ significantly from each other, we observed that in several instances CCI-injured animals only differed significantly from naïve animals and not from sham-operated rats. Sham-operated rats often showed an intermediate response compared with naïve and CCI-injured rats. In the open field, sham rats showed very similar behavior as the CCI-injured rats. This supports the hypothesis that sham-operated rats are not completely normal and underlines the importance of including naïve animals as a secondary control group. It has previously been shown that craniotomized animals can display behavioral deficits compared with naïve animals.[30]

CCI-injured rats exhibited an increased tendency to enter the center of the open field compared with controls, which may be due to disinhibition and impulsivity (common symptoms in TBI patients[51] and observed in rats following CCI-injury[52]) or decreased anxiety, which has been observed in CCI-injured mice.[53] Whereas the percent distance moved in the center of the open field was increased, the total distance moved and the mean velocity were not altered, indicating that there was no general hyperactivity in the CCI-injured animals. Several studies have observed increased thigmotaxis in an open field following experimental TBI in rodents, whereas some failed to observe a difference between TBI and sham-operated animals. Differences in observation might be explained by differences in injury type, location and severity, species and strain differences, and a different timing of the open field test.[53–57] Reduced anxiety-like behavior and increased disinhibition/impulsivity has been observed in other behavioral tests following CCI-injury, including elevated zero maze and light-dark box tests and the delay discounting task.[52,53]

CCI-injured rats exhibited anhedonia in the chronic period, which is an indication of depression-like behavior. Some studies have failed to observe anhedonia following experimental TBI in rodents, which could be due to differences in injury type, location and severity, species and strain differences, and a different timing of the sucrose preference test.[53,54]

Most of the EDs and seizures that we observed during this study were either spike-wave discharges (SWDs) or high-voltage rhythmic spike (HVRS) discharges and were bilateral in onset. If there was a behavioral manifestation, then it was usually a behavioral arrest. These SWDs and HVRS discharges have been shown to occur spontaneously in this and other rat strains (both inbred and outbred) and their occurrence progresses with age, which complicates the use of rodents to study acquired epilepsy.[58–60] Indeed, we also observed an increased frequency in EDs and seizures over time (from 6 to 9 months post-injury) in both sham-operated and CCI-injured rats, which suggest an aging effect that might have been slightly exacerbated by the CCI-injury (given the numerically higher frequency of EDs and seizures in this group). Unfortunately, we cannot confirm this aging effect in naïve rats, because none of the naïve rats were vEEG-monitored at both time-points for the occurrence of spontaneous epileptiform activity. Although some have argued that there is no difference in the occurrence of SWDs between sham-operated and FPI animals,[61] others have described a higher frequency of SWDs in FPI animals compared with shams.[62] In our study we did not observe a significant difference between naïve, sham-operated, and CCI-injured rats regarding the occurrence of EDs. There was, however, an increased frequency of behavioral seizures in CCI-injured rats compared with naïve rats at the final time-point.

Because of the controversy regarding SWDs, HVRS discharges, and non-convulsive (especially absence-like) seizures in models of post-traumatic epilepsy, we limit ourselves to the occurrence of convulsive (i.e., S3-5) seizures to make conclusions regarding the development of post-traumatic epilepsy (PTE) in our CCI rat model. At 6 months post-injury none of the rats had any convulsive seizures. At the 9-month time-point, one CCI-injured animal experienced two spontaneous convulsive seizures during the one-week monitoring period. This rat was considered epileptic and was also the only animal that went into *status epilepticus* during the subsequent PTZ test. It is important to note that this rat also had the highest frequency of spontaneous non-convulsive behavioral seizures during the one-week monitoring period at 9 months post-injury. Hence, 14% (1/7 vEEG-monitored) rats developed PTE by the end of our study, which is comparable to the study of Kelly and colleagues, who perceived spontaneous convulsive seizures in 15% of all CCI-injured rats (5% [2/40] in vEEG-monitored and 19% [17/88] in video-monitored rats).[63] The development of PTE has also been studied after CCI-injury in mice. Bolkvadze and Pitkänen observed spontaneous convulsive seizures in 9% of the CCI-injured mice,[64] whereas Hunt and colleagues reported that 13–18% of severely injured CCI mice had spontaneous convulsive seizures.[65,66] In our study one sham-operated rat experienced one convulsive seizure during the monitoring period, which is uncommon, but has been reported previously by others as well.[67] None of the naïve animals had convulsive seizures.

We observed a clear increase in seizure susceptibility during the second PTZ assay at 9 months post-injury when we used 30 mg/kg PTZ (86% CCI rats developed convulsive seizures vs. 38% controls), but not at 6 months post-injury with the 25 mg/kg PTZ dose. However, in a separate cohort (cohort 2), we also observed a clear increase in seizure susceptibility at 6 months post-injury when using the 30 mg/kg dose (78% CCI rats vs. 26% controls; similar to previous observations in CCI mice at this time-point[64]), suggesting that the dose of PTZ is important to distinguish between TBI animals and controls. Similar observations have been made by the group of Pitkänen, who also employed 25 mg/kg and 30 mg/kg PTZ doses in Sprague-Dawley rats to assess seizure susceptibility after TBI (FPI).[24,40]

An interesting observation in our study was the inverse relationship between the number of EDs and the latency to first convulsive seizure following PTZ administration. It seems that typically PTZ initially induces an increased frequency of EDs until a certain threshold is reached, which results in a convulsive seizure (usually a tonic-clonic S5 seizure). In animals that quickly experienced a convulsive seizure there was a low number of EDs, whereas in animals that experienced a convulsive seizure after a long time there was a high number of EDs. At 6 months, 25 mg/kg PTZ caused an increased number of EDs in CCI-injured rats, but hardly any convulsive seizures. At 9 months, 30 mg/kg PTZ caused convulsive seizures in many CCI-injured rats, which occurred relatively quickly after PTZ administration. At the same time, there were less EDs in this group during this test. A very strong relationship between the number of EDs and the latency to first convulsive seizure was observed at the subject level.

The CCI rats exhibited a clear deficit in the acquisition of the MWM task, which was most pronounced on day 2 of the training phase. Although the CCI-injured rats had a slower learning curve, they did not show a difference in escape latency and path length at the end of the acquisition phase compared with sham and naïve rats. So whereas CCI-injured rats were initially slower in learning the location of the platform, they managed to learn it equally well as the sham-operated and naïve rats by the end of the 8 days of the training period. In addition, they also displayed a slight non-significant deficit in the retention trial. Deficits in hippocampus-dependent spatial learning and memory have consistently been shown after experimental TBI in rodents using the MWM test.[68–70] Cognitive impairment following experimental TBI has been shown using several different paradigms, showing both retrograde and anterograde amnesia, as well as working memory deficits (reviewed in Whiting and colleagues[71]).

Correlation between subacute brain inflammation, microstructural alterations, lesion volume, and chronic TBI sequelae

Several correlations were observed between subacute TSPO expression and DTI metrics in ipsi- and contralesional brain regions (cortex and hippocampus) and long-term functional deficits. Importantly, not only the absolute [^{18}F]PBR111 SUVs and DTI values at the two subacute time-points correlated with chronic outcome, but also the relative change in TSPO expression and DTI parameters over time, that is, the dynamics of the neuroinflammatory response and degeneration/regeneration processes.

Surprisingly, a pronounced decrease in TSPO expression in the perilesional cortex over time correlated with a higher disinhibition level in CCI rats as suggested by the open field test. Interestingly, TSPO itself is involved in the synthesis of neurosteroids, some of which have anxiolytic effects (e.g., allopregnanolone). Overexpression of TSPO in mice has been shown to produce anxiolytic behavior.[72] Although no positive correlation could be established between the subacute increase in TSPO and the long-term increase in disinhibition, it cannot be excluded that TSPO played some role in the subsequent disinhibited behavior. CCI animals with an increase in FA in ipsilesional hippocampus over time showed less disinhibition than animals where the initial FA deficit did not resolve or even worsened over time. An increase in FA might indicate neuronal regeneration and repair, which may explain the better functional outcome.[47,73] Johnstone and colleagues observed increased fractional anisotropy in the chronic period following FPI and speculated that this may be related to structural reorganization,

which may have explained the recovery of neuronal responsiveness that they observed.[48] Similarly, in our study, the increased FA may reflect structural reorganization that is responsible for the better functional outcome on this test.

High levels of subacute TSPO in the ipsilesional hippocampus and perilesional cortex correlated with high spontaneous behavioral seizure frequency and increased seizure susceptibility at 6 and 9 months post-TBI. Animals that had a minimal decrease in TSPO binding over time, that is, persistent inflammation, were shown to have a high frequency of behavioral seizures and increased seizure susceptibility at 9 months post-TBI. Interestingly, the only rat that developed spontaneous recurrent convulsive seizures in this study and that went into *status epilepticus* following PTZ administration at the final time-point was also the only animal that had a prominent increase in subacute TSPO expression over time in the perilesional cortex.

Several inflammatory mediators have been implicated in epileptogenesis, seizure initiation, and TBI-induced pathogenesis and might play a role in the development of PTE (reviewed in Webster and associates[7]). A pronounced and enduring inflammatory response following TBI might lead to the development of PTE, as supported by our study. Changes in FA, MD, AD, and RD also correlated with increased seizure susceptibility. A more pronounced deficit in FA, MD, AD, and RD in perilesional cortex correlated with a shorter latency to the first spike during the 6-month PTZ assay. Our observations are in line with studies performed by Kharatishvili and Immonen and colleagues, who showed that increased average diffusion in ipsilesional hippocampus and perilesional cortex correlated with increased chronic seizure susceptibility after FPI (latency to first spike, number of spikes, and number of EDs) and with the severity of mossy fiber sprouting post-FPI, a form of hippocampal circuitry reorganization that is thought to be related to epileptogenesis.[24,25] This indicates that these diffusion measurements can be good predictors of seizure susceptibility in different TBI models. CCI rats with a limited increase or even a decrease in FA over time in ipsilesional hippocampus had a higher number of EDs during the PTZ assay at 6 months post-injury, whereas a more pronounced increase in FA in perilesional cortex over time correlated with a shorter latency to the first convulsive seizure during the 9-month PTZ assay. An increase in FA can be due to increased plasticity/structural reorganization (beneficial or aberrant) or increased organized gliosis (e.g., glial scarring).[48,49]

A pronounced subacute neuroinflammatory response in the perilesional cortex correlated with a more severe learning deficit in our CCI rats. Part of the lesioned and perilesional cortex is the parietal association cortex, which is implicated in spatial processing. Lesions of this area have been shown to cause deficits in the acquisition of the MWM task.[74] Neuroinflammation has been shown to affect cognition; inhibition of subacute inflammation has been demonstrated to improve the cognitive outcome following experimental TBI.[9–11] CCI rats with a more pronounced increase in MD and RD in ipsilesional hippocampus at 18 days post-injury displayed a greater deficit in the acquisition of the MWM task. Similarly, Immonen and colleagues showed that FPI rats with a higher increase in average diffusion in ipsilesional hippocampus at 23 days post-injury exhibited a greater impairment in the MWM test at 7 months post-injury.[26] This research group also observed a correlation between average diffusion in hippocampus at several acute and chronic time-points post-FPI and mossy fiber sprouting at a chronic time-point.[24] Interestingly, inhibition of mossy fiber sprouting has been shown to coincide with an amelioration of MWM performance in pilocarpine-treated mice.[75]

The interpretation of diffusion metrics remains challenging, because various cellular alterations can cause a similar DTI abnormality. In addition, several cellular processes (increased plasticity, gliosis) can have both beneficial and detrimental effects, possibly affecting different behavioral processes in a different manner.

Interestingly, not only the pronounced changes in TSPO expression and microstructure in the ipsilesional brain regions correlated with the chronic outcome, but also the variability in these parameters in the contralesional brain regions correlated well with the long-term deficits.

Surprisingly, the lesion volume only correlated with seizure susceptibility at 6 months post-injury and not with any other chronic deficit. A bigger lesion in the subacute phase correlated with an increased seizure susceptibility at this time-point. Bigger lesion volumes have been shown to be associated with a worse outcome after TBI.[28]

Prognostic biomarkers and models

ROC curve analysis showed that certain specific TSPO PET and DTI parameters had good sensitivity and specificity (AUC = 0.85–1.00) to distinguish between traumatized rats with and without a particular chronic deficit and hence are very promising prognostic biomarkers for the long-term outcome following TBI.

Stepwise regression analysis showed that both TSPO PET and DTI data alone, as well as the combination of TSPO PET and DTI parameters provided good regression models (adjusted $R^2 = 0.54$–1.00) to explain the variability in the chronic outcome parameters, depending on which behavioral parameter was investigated. DTI parameters could predict all investigated chronic deficits. TSPO PET parameters could also predict several of the investigated TBI sequelae. In several cases, combining TSPO PET and DTI parameters resulted in the best prognostic models. Adding lesion size as a predictor to these models did not improve them. The TSPO PET and DTI measurements seem to provide more information about the underlying biological processes that ultimately lead to the development of these chronic deficits and are better predictors of the long-term outcome than the lesion volume. These data indicate that both TSPO PET and DTI parameters could be useful characteristics to be implemented into novel, improved prognostic models for the outcome of TBI. Moreover, these models may give a more precise prognosis than the current prognostic models. More research is warranted to conclude whether such prognostic models would be of value to predict the outcome of individual subjects.

An interesting study by Shultz and colleagues investigated the potential of several neuroimaging ([^{18}F]FDG PET and T_2-weighted MRI) and behavioral assessments as possible predictors of PTE in an FPI rat model. Of all the investigated parameters, only measurements of glucose metabolism (using FDG PET) in the ipsilesional hippocampus at different time-points after TBI were able to predict the epileptic outcome in this model. In addition, they observed hippocampal deformation (assessed by large-deformation high-dimensional mapping of hippocampal morphometry) in the subacute phase that was different between epileptic and non-epileptic TBI rats. All investigated MRI parameters (including volumetric and MRI intensity analyses of several brain regions) failed to predict epilepsy outcome.[76] Based on these and our observations, it would be useful to investigate and compare (1) brain inflammation (using TSPO PET), (2) microstructural changes (using DTI), and (3) hypometabolism (using FDG PET) as potential predictors of PTE and other chronic TBI outcomes in a single study

to be able to draw conclusions regarding their respective prognostic potential and potentially added value. Interestingly, Yu and colleagues have compared TSPO PET imaging with FDG PET imaging in a FPI rat model and concluded that TSPO PET was much more sensitive for the detection of post-traumatic pathologies than FDG PET.[17] However, whether TSPO imaging has a better prognostic value for chronic TBI outcome than FDG imaging needs yet to be confirmed.

Limitations of our study

A limitation of our study is that MRI and PET scans were not performed on the same days in the animals (e.g., both on day 7 and day 21 post-injury), which would have allowed a better comparison between DTI and TSPO PET data. Unfortunately, this was not possible in our study for logistic reasons. Moreover, it is not good for animals to be anesthetized for a long time or on consecutive days. The animals need to recover in between consecutive ''anesthesia sessions'' (i.e., surgery [trauma induction], MRI, and PET scanning sessions), especially shortly after TBI. For this reason, we chose to perform the first MRI scanning session on day 4 after trauma induction and the first PET scanning session on day 7 (based on the peak of TSPO expression that was previously reported in the literature). Advances in combined pre-clinical PET/MR imaging will eventually help to solve these issues and allow for the performance of PET and MRI together in one (overall shorter) scanning session.

A second limitation of our study is the rather short vEEG monitoring periods. Monitoring the animals for a longer time would have increased the chance of detecting additional spontaneous convulsive seizures. However, because the incidence of PTE in our study is similar to the one reported by Kelly and associates,[63] we believe that the observed incidence is not an underestimation.

Conclusion

Our study shows that subacute neuroinflammation, measured by PET imaging with a TSPO radioligand, and microstructural changes, measured by DTI, correlate with several chronic deficits after CCI-injury in rats, including disinhibition, spontaneous behavioral seizure frequency, seizure susceptibility, and impaired visuospatial learning. Not just the robust alterations in brain inflammation and microstructure in the ipsilesional hemisphere correlated well with chronic TBI sequelae, but also the variability in TSPO expression and DTI metrics in the contralesional hemisphere. Importantly, not only the absolute PET/DTI values at the two subacute time-points correlated with chronic outcome, but also the subacute evolution of brain inflammation and microstructural changes proved to be good correlates of long-term functional deficits. Combining TSPO PET and DTI seemed to have an added value in the prediction of some chronic deficits. Overall, our study suggests that TSPO PET/DTI parameters could be useful prognostic biomarkers and be implemented in novel, improved prognostic models for prediction of the development of different TBI sequelae.

Acknowledgments

We thank Krystyna Szewczyk, Annemie Van Eetveldt, Philippe Joye, and Caroline Berghmans for their excellent technical assistance. This research was supported by ERA-NET NEURON/Research Foundation Flanders GA00913N. Stephan Missault has a PhD fellowship from the Research Foundation Flanders (11K371 4N/11K3716N). The 7T PharmaScan MR system was purchased through Hercules Foundation funding (Belgium) under the promotership of Prof. Annemie Van der Linden. We also acknowledge the Interuniversity Poles of Attraction of the Belgian Federal Science Policy Office (IAP7/16), Belgian Alzheimer Research Foundation (SAO-FRA), agreement between Institute Born-Bunge and University of Antwerp, the Medical Research Foundation Antwerp, the Thomas Riellaerts Research Fund, the Alzheimer Research Center Groningen (UMCG), and Neurosearch Antwerp.

Author Disclosure Statement

No competing financial interests exist.

References

1. Roozenbeek, B., Maas, A.I., and Menon, D.K. (2013). Changing patterns in the epidemiology of traumatic brain injury. Nat. Rev. Neurol. 9, 231–236.
2. Bramlett, H.M., and Dietrich, W.D. (2015). Long-term consequences of traumatic brain injury: current status of potential mechanisms of injury and neurological outcomes. J. Neurotrauma 32, 1834–1848.
3. MRC CRASH Trial Collaborators, Perel, P., Arango, M., Clayton, T., Edwards, P., Komolafe, E., Poccock, S., Roberts, I., Shakur, H., Steyerberg, E., and Yutthakasemsunt, S. (2008). Predicting outcome after traumatic brain injury: practical prognostic models based on large cohort of international patients. BMJ 336, 425–429.
4. Steyerberg, E.W., Mushkudiani, N., Perel, P., Butcher, I., Lu, J., McHugh, G.S., Murray, G.D., Marmarou, A., Roberts, I., Habbema, J.D., and Maas, A.I. (2008). Predicting outcome after traumatic brain injury: development and international validation of prognostic scores based on admission characteristics. PLoS Med 5, e165; discussion e165.
5. Maas, A.I., Marmarou, A., Murray, G.D., Teasdale, S.G., and Steyerberg, E.W. (2007). Prognosis and clinical trial design in traumatic brain injury: the IMPACT study. J. Neurotrauma 24, 232–238.
6. Young, N.H., and Andrews, P.J. (2008). Developing a prognostic model for traumatic brain injury—a missed opportunity? PLoS Med 5, e168.
7. Webster, K.M., Sun, M., Crack, P., O'Brien, T.J., Shultz, S.R., and Semple, B.D. (2017). Inflammation in epileptogenesis after traumatic brain injury. J. Neuroinflammation 14, 10.
8. Russo, M.V., and McGavern, D.B. (2016). Inflammatory neuroprotection following traumatic brain injury. Science 353, 783–785.
9. James, M.L., Wang, H., Cantillana, V., Lei, B., Kernagis, D.N., Dawson, H.N., Klaman, L.D., and Laskowitz, D.T. (2012). TT-301 inhibits microglial activation and improves outcome after central nervous system injury in adult mice. Anesthesiology 116, 1299–1311.
10. Clausen, F., Hanell, A., Bjork, M., Hillered, L., Mir, A.K., Gram, H., and Marklund, N. (2009). Neutralization of interleukin-1beta modifies the inflammatory response and improves histological and cognitive outcome following traumatic brain injury in mice. Eur. J. Neurosci. 30, 385–396.
11. Lloyd, E., Somera-Molina, K., Van Eldik, L.J., Watterson, D.M., and Wainwright, M.S. (2008). Suppression of acute proinflammatory cytokine and chemokine upregulation by post-injury administration of a novel small molecule improves long-term neurologic outcome in a mouse model of traumatic brain injury. J. Neuroinflammation 5, 28.
12. Juengst, S.B., Kumar, R.G., Failla, M.D., Goyal, A., and Wagner, A.K. (2015). Acute inflammatory biomarker profiles predict depression risk following moderate to severe traumatic brain injury. J. Head Trauma Rehabil. 30, 207–218.
13. Witcher, K.G., Eiferman, D.S., and Godbout, J.P. (2015). Priming the inflammatory pump of the CNS after traumatic brain injury. Trends Neurosci. 38, 609–620.
14. Fenn, A.M., Gensel, J.C., Huang, Y., Popovich, P.G., Lifshitz, J., and Godbout, J.P. (2014). Immune activation promotes depression 1 month after diffuse brain injury: a role for primed microglia. Biol. Psychiatry 76, 575–584.
15. Bertoglio, D., Verhaeghe, J., Santermans, E., Amhaoul, H., Jonckers, E., Wyffels, L., Van Der Linden, A., Hens, N., Staelens, S., and Dedeurwaerdere, S. (2017). Non-invasive PET imaging of brain inflammation at disease onset predicts spontaneous recurrent seizures and reflects comorbidities. Brain Behav. Immun. 61, 69–79.
16. Wang, Y., Yue, X., Kiesewetter, D.O., Niu, G., Teng, G., and Chen, X. (2014). PET imaging of neuroinflammation in a rat traumatic brain

injury model with radiolabeled TSPO ligand DPA-714. Eur. J. Nucl. Med. Mol. Imaging 41, 1440–1449.
17. Yu, I., Inaji, M., Maeda, J., Okauchi, T., Nariai, T., Ohno, K., Higuchi, M., and Suhara, T. (2010). Glial cell-mediated deterioration and repair of the nervous system after traumatic brain injury in a rat model as assessed by positron emission tomography. J. Neurotrauma 27, 1463–1475.
18. Roncaroli, F., Su, Z., Herholz, K., Gerhard, A., and Turkheimer, F.E. (2016). TSPO expression in brain tumours: is TSPO a target for brain tumour imaging? Clin. Transl. Imaging 4, 145–156.
19. Donat, C.K., Gaber, K., Meixensberger, J., Brust, P., Pinborg, L.H., Hansen, H.H., and Mikkelsen, J.D. (2016). Changes in binding of [(123)I]CLINDE, a high-affinity translocator protein 18 kDa (TSPO) selective radioligand in a rat model of traumatic brain injury. Neuromolecular Med. 18, 158–169.
20. Irimia, A., Wang, B., Aylward, S.R., Prastawa, M.W., Pace, D.F., Gerig, G., Hovda, D.A., Kikinis, R., Vespa, P.M., and Van Horn, J.D. (2012). Neuroimaging of structural pathology and connectomics in traumatic brain injury: Toward personalized outcome prediction. Neuroimage Clin. 1, 1–17.
21. Koerte, I.K., Hufschmidt, J., Muehlmann, M., Lin, A.P., and Shenton, M.E. (2016). Advanced neuroimaging of mild traumatic brain injury, in: *Translational Research in Traumatic Brain Injury*. D. Laskowitz, and G. Grant. (eds). Boca Raton (FL).
22. Wright, D.K., Johnston, L.A., Kershaw, J., Ordidge, R., O'Brien, T.J., and Shultz, S.R. (2017). Changes in apparent fiber density and track-weighted imaging metrics in white matter following experimental traumatic brain injury. J. Neurotrauma 34, 2109–2118.
23. Wright, D.K., Trezise, J., Kamnaksh, A., Bekdash, R., Johnston, L.A., Ordidge, R., Semple, B.D., Gardner, A.J., Stanwell, P., O'Brien, T.J., Agoston, D.V., and Shultz, S.R. (2016). Behavioral, blood, and magnetic resonance imaging biomarkers of experimental mild traumatic brain injury. Sci. Rep. 6, 28713.
24. Kharatishvili, I., Immonen, R., Grohn, O., and Pitkanen, A. (2007). Quantitative diffusion MRI of hippocampus as a surrogate marker for post-traumatic epileptogenesis. Brain 130, 3155–3168.
25. Immonen, R., Kharatishvili, I., Grohn, O., and Pitkanen, A. (2013). MRI biomarkers for post-traumatic epileptogenesis. J. Neurotrauma 30, 1305–1309.
26. Immonen, R.J., Kharatishvili, I., Grohn, H., Pitkanen, A., and Grohn, O.H. (2009). Quantitative MRI predicts long-term structural and functional outcome after experimental traumatic brain injury. Neuroimage 45, 1–9.
27. Frey, L., Lepkin, A., Schickedanz, A., Huber, K., Brown, M.S., and Serkova, N. (2014). ADC mapping and T1-weighted signal changes on post-injury MRI predict seizure susceptibility after experimental traumatic brain injury. Neurol. Res. 36, 26–37.
28. Chastain, C.A., Oyoyo, U.E., Zipperman, M., Joo, E., Ashwal, S., Shutter, L.A., and Tong, K.A. (2009). Predicting outcomes of traumatic brain injury by imaging modality and injury distribution. J. Neurotrauma 26, 1183–1196.
29. Missault, S., Peeters, L., Amhaoul, H., Thomae, D., Van Eetveldt, A., Favier, B., Thakur, A., Van Soom, J., Pitkanen, A., Augustyns, K., Joossens, J., Staelens, S., and Dedeurwaerdere, S. (2017). Decreased levels of active uPA and KLK8 assessed by [111 In]MICA-401 binding correlate with the seizure burden in an animal model of temporal lobe epilepsy. Epilepsia 58, 1615–1625.
30. Cole, J.T., Yarnell, A., Kean, W.S., Gold, E., Lewis, B., Ren, M., McMullen, D.C., Jacobowitz, D.M., Pollard, H.B., O'Neill, J.T., Grunberg, N.E., Dalgard, C.L., Frank, J.A., and Watson, W.D. (2011). Craniotomy: true sham for traumatic brain injury, or a sham of a sham? J. Neurotrauma 28, 359–369.
31. Bourdier, T., Pham, T.Q., Henderson, D., Jackson, T., Lam, P., Izard, M., and Katsifis, A. (2012). Automated radiosynthesis of [18F]PBR111 and [18F]PBR102 using the Tracerlab FXFN and Tracerlab MXFDG module for imaging the peripheral benzodiazepine receptor with PET. Appl. Radiat. Isot. 70, 176–183.
32. Katsifis, A., Loc'h, C., Henderson, D., Bourdier, T., Pham, T., Greguric, I., Lam, P., Callaghan, P., Mattner, F., Eberl, S., and Fulham, M. (2011). A rapid solid-phase extraction method for measurement of non-metabolised peripheral benzodiazepine receptor ligands, [(18)F]PBR102 and [(18)F]PBR111, in rat and primate plasma. Nucl. Med. Biol. 38, 137–148.
33. Hudson, H.M., and Larkin, R.S. (1994). Accelerated image reconstruction using ordered subsets of projection data. IEEE Trans. Med. Imaging 13, 601–609.
34. Defrise, M., Kinahan, P.E., Townsend, D.W., Michel, C., Sibomana, M., and Newport, D.F. (1997). Exact and approximate rebinning algorithms for 3-D PET data. IEEE Trans. Med. Imaging 16, 145–158.
35. Tu, T.W., Turtzo, L.C., Williams, R.A., Lescher, J.D., Dean, D.D., and Frank, J.A. (2014). Imaging of spontaneous ventriculomegaly and vascular malformations in Wistar rats: implications for preclinical research. J. Neuropathol. Exp. Neurol. 73, 1152–1165.
36. Missault, S., Van den Eynde, K., Vanden Berghe, W., Fransen, E., Weeren, A., Timmermans, J.P., Kumar-Singh, S., and Dedeurwaerdere, S. (2014). The risk for behavioural deficits is determined by the maternal immune response to prenatal immune challenge in a neurodevelopmental model. Brain Behav. Immun. 42, 138–146.
37. Amhaoul, H., Hamaide, J., Bertoglio, D., Reichel, S.N., Verhaeghe, J., Geerts, E., Van Dam, D., De Deyn, P.P., Kumar-Singh, S., Katsifis, A., Van Der Linden, A., Staelens, S., and Dedeurwaerdere, S. (2015). Brain inflammation in a chronic epilepsy model: evolving pattern of the translocator protein during epileptogenesis. Neurobiol. Dis. 82, 526–539.
38. Amhaoul, H., Ali, I., Mola, M., Van Eetveldt, A., Szewczyk, K., Missault, S., Bielen, K., Kumar-Singh, S., Rech, J., Lord, B., Ceusters, M., Bhattacharya, A., and Dedeurwaerdere, S. (2016). P2X7 receptor antagonism reduces the severity of spontaneous seizures in a chronic model of temporal lobe epilepsy. Neuropharmacology 105, 175–185.
39. Fisher, R.S. (2015). Redefining epilepsy. Curr. Opin. Neurol. 28, 130–135.
40. Huusko, N., Romer, C., Ndode-Ekane, X.E., Lukasiuk, K., and Pitkanen, A. (2015). Loss of hippocampal interneurons and epileptogenesis: a comparison of two animal models of acquired epilepsy. Brain Struct. Funct. 220, 153–191.
41. van der Werf, I.M., Van Dam, D., Missault, S., Yalcin, B., De Deyn, P.P., Vandeweyer, G., and Kooy, R.F. (2017). Behavioural characterization of AnkyrinG deficient mice, a model for ANK3 related disorders. Behav. Brain Res. 328, 218–226.
42. Van den Eynde, K., Missault, S., Fransen, E., Raeymaekers, L., Willems, R., Drinkenburg, W., Timmermans, J.P., Kumar-Singh, S., and Dedeurwaerdere, S. (2014). Hypolocomotive behaviour associated with increased microglia in a prenatal immune activation model with relevance to schizophrenia. Behav. Brain Res. 258, 179–186.
43. Mizrahi, R., Rusjan, P.M., Kennedy, J., Pollock, B., Mulsant, B., Suridjan, I., De Luca, V., Wilson, A.A., and Houle, S. (2012). Translocator protein (18 kDa) polymorphism (rs6971) explains in-vivo brain binding affinity of the PET radioligand [(18)F]-FEPPA. J. Cereb. Blood Flow Metab. 32, 968–972.
44. Owen, D.R., Yeo, A.J., Gunn, R.N., Song, K., Wadsworth, G., Lewis, A., Rhodes, C., Pulford, D.J., Bennacef, I., Parker, C.A., StJean, P.L., Cardon, L.R., Mooser, V.E., Matthews, P.M., Rabiner, E.A., and Rubio, J.P. (2012). An 18-kDa translocator protein (TSPO) polymorphism explains differences in binding affinity of the PET radioligand PBR28. J. Cereb. Blood Flow Metab. 32, 1–5.
45. Albrecht, D.S., Granziera, C., Hooker, J.M., and Loggia, M.L. (2016). In vivo imaging of human neuroinflammation. ACS Chem. Neurosci. 7, 470–483.
46. Lyoo, C.H., Ikawa, M., Liow, J.S., Zoghbi, S.S., Morse, C.L., Pike, V.W., Fujita, M., Innis, R.B., and Kreisl, W.C. (2015). Cerebellum can serve as a pseudo-reference region in Alzheimer disease to detect neuroinflammation measured with PET radioligand binding to translocator protein. J. Nucl. Med. 56, 701–706.
47. Hutchinson, E.B., Schwerin, S.C., Avram, A.V., Juliano, S.L., and Pierpaoli, C. (2017). Diffusion MRI and the detection of alterations following traumatic brain injury. J. Neurosci. Res. 96, 612–625.
48. Johnstone, V.P., Wright, D.K., Wong, K., O'Brien, T.J., Rajan, R., and Shultz, S.R. (2015). Experimental traumatic brain injury results in long-term recovery of functional responsiveness in sensory cortex but persisting structural changes and sensorimotor, cognitive, and emotional deficits. J. Neurotrauma 32, 1333–1346.
49. Budde, M.D., Janes, L., Gold, E., Turtzo, L.C., and Frank, J.A. (2011). The contribution of gliosis to diffusion tensor anisotropy and tractography following traumatic brain injury: validation in the rat using Fourier analysis of stained tissue sections. Brain 134, 2248–2260.
50. Immonen, R.J., Kharatishvili, I., Niskanen, J.P., Grohn, H., Pitkanen, A., and Grohn, O.H. (2009). Distinct MRI pattern in lesional and perilesional area after traumatic brain injury in rat–11 months follow-up. Exp. Neurol. 215, 29–40.
51. Kocka, A., and Gagnon, J. (2014). Definition of impulsivity and related terms following traumatic brain injury: a review of the different concepts and measures used to assess impulsivity, disinhibition and other related concepts. Behav. Sci. (Basel) 4, 352–370.

52. Vonder Haar, C., Martens, K.M., Riparip, L.K., Rosi, S., Wellington, C.L., and Winstanley, C.A. (2017). Frontal Traumatic Brain Injury Increases Impulsive Decision Making in Rats: A Potential Role for the Inflammatory Cytokine Interleukin-12. J Neurotrauma 34, 2790–2800.
53. Tucker, L.B., Burke, J.F., Fu, A.H., and McCabe, J.T. (2017). Neuropsychiatric symptom modeling in male and female C57BL/6J mice after experimental traumatic brain injury. J. Neurotrauma 34, 890–905.
54. Jones, N.C., Cardamone, L., Williams, J.P., Salzberg, M.R., Myers, D., and O'Brien, T.J. (2008). Experimental traumatic brain injury induces a pervasive hyperanxious phenotype in rats. J. Neurotrauma 25, 1367–1374.
55. Kim, H., Yu, T., Cam-Etoz, B., van Groen, T., Hubbard, W.J., and Chaudry, I.H. (2017). Treatment of traumatic brain injury with 17alpha-ethinylestradiol-3-sulfate in a rat model. J. Neurosurg. 127, 23–31.
56. McNamara, K.C., Lisembee, A.M., and Lifshitz, J. (2010). The whisker nuisance task identifies a late-onset, persistent sensory sensitivity in diffuse brain-injured rats. J. Neurotrauma 27, 695–706.
57. Rowe, R.K., Ziebell, J.M., Harrison, J.L., Law, L.M., Adelson, P.D., and Lifshitz, J. (2016). Aging with traumatic brain injury: effects of age at injury on behavioral outcome following diffuse brain injury in rats. Dev. Neurosci. 38, 195–205.
58. Kelly, K.M. (2004). Spike-wave discharges: absence or not, a common finding in common laboratory rats. Epilepsy Curr. 4, 176–177.
59. Pearce, P.S., Friedman, D., Lafrancois, J.J., Iyengar, S.S., Fenton, A.A., Maclusky, N.J., and Scharfman, H.E. (2014). Spike-wave discharges in adult Sprague-Dawley rats and their implications for animal models of temporal lobe epilepsy. Epilepsy Behav. 32, 121–131.
60. Shaw, F.Z. (2004). Is spontaneous high-voltage rhythmic spike discharge in Long Evans rats an absence-like seizure activity? J. Neurophysiol. 91, 63–77.
61. Rodgers, K.M., Dudek, F.E., and Barth, D.S. (2015). Progressive, Seizure-like, spike-wave discharges are common in both injured and uninjured Sprague-Dawley Rats: implications for the fluid percussion injury model of post-traumatic epilepsy. J. Neurosci. 35, 9194–9204.
62. Sick, T., Wasserman, J., Bregy, A., Sick, J., Dietrich, W.D., and Bramlett, H.M. (2017). Increased expression of epileptiform spike/wave discharges one year after mild, moderate, or severe fluid percussion brain injury in rats. J. Neurotrauma 34, 2467–2474.
63. Kelly, K.M., Miller, E.R., Lepsveridze, E., Kharlamov, E.A., and McHedlishvili, Z. (2015). Posttraumatic seizures and epilepsy in adult rats after controlled cortical impact. Epilepsy Res. 117, 104–116.
64. Bolkvadze, T., and Pitkanen, A. (2012). Development of post-traumatic epilepsy after controlled cortical impact and lateral fluid-percussion-induced brain injury in the mouse. J. Neurotrauma 29, 789–812.
65. Hunt, R.F., Scheff, S.W., and Smith, B.N. (2009). Posttraumatic epilepsy after controlled cortical impact injury in mice. Exp. Neurol. 215, 243–252.
66. Hunt, R.F., Scheff, S.W., and Smith, B.N. (2010). Regionally localized recurrent excitation in the dentate gyrus of a cortical contusion model of posttraumatic epilepsy. J. Neurophysiol. 103, 1490–1500.
67. Nissinen, J., Andrade, P., Natunen, T., Hiltunen, M., Malm, T., Kanninen, K., Soares, J.I., Shatillo, O., Sallinen, J., Ndode-Ekane, X.E., and Pitkanen, A. (2017). Disease-modifying effect of atipamezole in a model of post-traumatic epilepsy. Epilepsy Res. 136, 18–34.
68. Hamm, R.J., Dixon, C.E., Gbadebo, D.M., Singha, A.K., Jenkins, L.W., Lyeth, B.G., and Hayes, R.L. (1992). Cognitive deficits following traumatic brain injury produced by controlled cortical impact. J. Neurotrauma 9, 11–20.
69. Scheff, S.W., Baldwin, S.A., Brown, R.W., and Kraemer, P.J. (1997). Morris water maze deficits in rats following traumatic brain injury: lateral controlled cortical impact. J. Neurotrauma 14, 615–627.
70. Smith, D.H., Okiyama, K., Thomas, M.J., Claussen, B., and McIntosh, T.K. (1991). Evaluation of memory dysfunction following experimental brain injury using the Morris water maze. J. Neurotrauma 8, 259–269.
71. Whiting, M.D., Baranova, A.I., and Hamm, R.J. (2006). Cognitive impairment following traumatic brain injury, in: *Animal Models of Cognitive Impairment*. E.D. Levin, and J.J. Buccafusco (eds). Boca Raton (FL).
72. Li, L., Wang, W., Zhang, L.M., Jiang, X.Y., Sun, S.Z., Sun, L.J., Guo, Y., Gong, J., Zhang, Y.Z., Wang, H.L., and Li, Y.F. (2017). Over-expression of the 18 kDa translocator protein (TSPO) in the hippocampal dentate gyrus produced anxiolytic and antidepressant-like behavioural effects. Neuropharmacology 125, 117–128.
73. Wang, S., Chopp, M., Nazem-Zadeh, M.R., Ding, G., Nejad-Davarani, S.P., Qu, C., Lu, M., Li, L., Davoodi-Bojd, E., Hu, J., Li, Q., Mahmood, A., and Jiang, Q. (2013). Comparison of neurite density measured by MRI and histology after TBI. PLoS One 8, e63511.
74. Save, E., and Moghaddam, M. (1996). Effects of lesions of the associative parietal cortex on the acquisition and use of spatial memory in egocentric and allocentric navigation tasks in the rat. Behav. Neurosci. 110, 74–85.
75. Ikegaya, Y., Nishiyama, N., and Matsuki, N. (2000). L-type Ca(2+) channel blocker inhibits mossy fiber sprouting and cognitive deficits following pilocarpine seizures in immature mice. Neuroscience 98, 647–659.
76. Shultz, S.R., Cardamone, L., Liu, Y.R., Hogan, R.E., Maccotta, L., Wright, D.K., Zheng, P., Koe, A., Gregoire, M.C., Williams, J.P., Hicks, R.J., Jones, N.C., Myers, D.E., O'Brien, T.J., and Bouilleret, V. (2013). Can structural or functional changes following traumatic brain injury in the rat predict epileptic outcome? Epilepsia 54, 1240–1250.

Address correspondence to:
Stephan Missault, PhD
University of Antwerp
Universiteitsplein 1
2610 Wilrijk
Belgium

E-mail: stephan.missault@uantwerpen.be